3
Strategic Anion Templation for the Assembly of Interlocked Structures

Michał J. Chmielewski and Paul D. Beer

3.1
Introduction

Anions are usually perceived as elusive species, difficult to trap and thus presenting a particular challenge to supramolecular chemists aiming at the design of efficient anion receptors [1]. Low charge densities (in comparison with isoelectronic cations) and high solvation energies are traditionally blamed for their sometimes disappointingly weak interactions with synthetic receptors. This, together with their weakly pronounced coordination preferences, is why anions may have been overlooked as potential templates.

However, an increasing body of evidence now seems to indicate [2] that although these limitations certainly exist, they are of a less fundamental nature then previously thought and may be overcome by improved receptor design. Continuing progress in the construction of anion receptors has resulted in the development of simple, organic, hydrogen bond donating units that exhibit strong affinities towards anions. Furthermore, these affinities are solvent dependent and sometimes it is enough to use a less competitive solvent to achieve the desired strength of binding. Strong binding in turn is a prerequisite for the use of anions as templates in the supramolecular assembly processes.

Over the past few years, numerous, often serendipitous, discoveries of anion templating phenomena have demonstrated that the potential of using anions as templates was underestimated [2]. In this chapter, we wish to illustrate that by systematic and rational research this potential can be developed into a highly effective strategy, which compares favorably with previous approaches based on cationic and neutral templating agents. More specifically, the use of anion recognition for the formation of pseudorotaxanes, rotaxanes and catenanes will be described, with emphasis placed on recent work of our group on the use of halide anions as templates in the formation of new architectures with sensory properties [3].

Organic Nanostructures. Edited by Jerry L. Atwood and Jonathan W. Steed
Copyright © 2008 WILEY-VCH Verlag GmbH & Co. KGaA, Weinheim
ISBN: 978-3-527-31836-0

Our motivations for carrying out this work were twofold. First, we wanted to explore the scope and limitations of anion templation as a novel method for the construction of interpenetrated structures. Second, such interlocked structures, after template removal, may act as hosts for anionic guests by virtue of their unique, topologically constrained three-dimensional cavities with orthogonal alignment of binding units. We hoped that a high degree of preorganization in the receptors' three-dimensional cleft and complete encapsulation of anions would lead to strong association and high selectivity in anion binding. Indeed, the only literature precedent, a pyrrole amide-based catenane by Sessler, Vögtle and coworkers [4], exhibits binding characteristics that compares favorably with a macrocyclic control. Unfortunately, this catenane was obtained in just 4% yield and attempts to improve the yield by anion templation were unsuccessful.

Three-dimensional cavities of rotaxanes and catenanes appear even more appealing in the context of difficulties afflicting two-dimensional receptors [5]. Acyclic clefts and macrocycles, which dominate the current landscape of anion receptors, often suffer from poor selectivities. It is becoming more and more apparent that, despite synthetic difficulties, they need to be elaborated into three-dimensional receptors able to embrace anions fully, in order to overcome this issue. Traditional approaches towards this goal may be exemplified by the construction of cryptands [6] or lariat-type compounds [7]. Alternatively, one may thread a one-dimensional, acyclic receptor through the annulus of a two-dimensional, macrocyclic receptor, thus creating a three-dimensional cavity for anion recognition. Such a design has a number of potential advantages, such as the aforementioned orthogonal disposition of the two binding units, which is difficult to achieve by other means, lower risk of slow exchange kinetics owing to less rigid, mechanically bound structure than that of covalently linked polycyclic cage compounds and a number of potential mechanisms of signal transduction, based on anion-induced change in co-conformation or in mutual interactions between thread and macrocycle. Thus we believe that rotaxanes and catenanes have huge potential in anion recognition and sensing.

3.2
Precedents of Anion-directed Formation of Interwoven Architectures

Two key types of self-assembly have been employed in the construction of interwoven molecules (Figure 3.1). In the first, a discrete interweaving template [8] is used to direct complex formation. In this case, the template is not a part of any component and may be removed from the interlocked system following synthesis. The archetypical example of such an approach is provided by the seminal work of Sauvage and coworkers, who used Cu(I) metal cations to control the formation of a wide range of interlocked species, including the [2]catenane illustrated [9]. Alternatively, the assembly may be driven by direct interaction between the components leading to the reversible formation of a precursor complex, which is then "trapped" by covalent bond formation to give a permanently interlocked system. This strategy, dubbed by

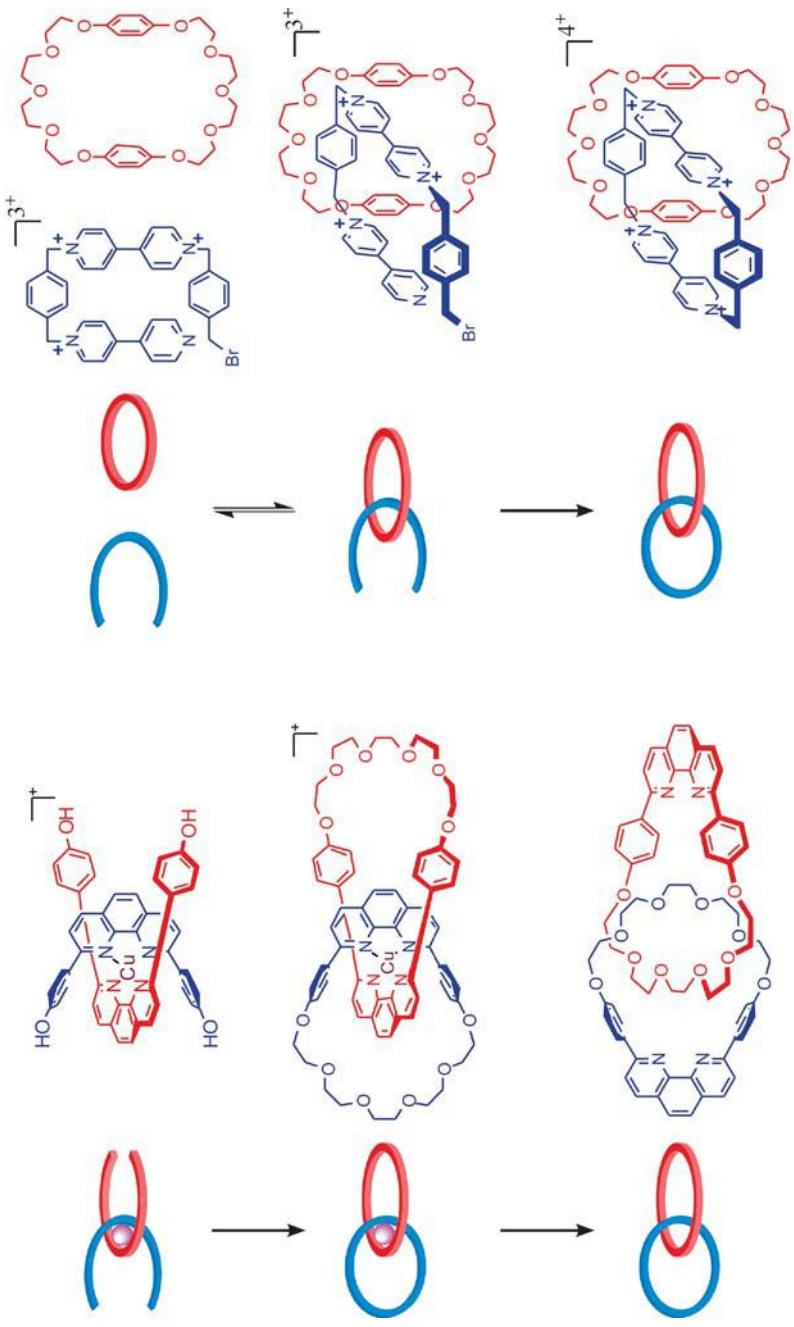

Figure 3.1 Two methods of generating interlocked architectures: template-directed assembly of orthogonal precursor complex (left) and structure-directed self-assembly (right).

Stoddart "structure-driven self-assembly" [10], is exemplified by his catenane synthesis [11], guided by attractive π–π interactions.

All previous applications of anion recognition in the synthesis of interlocked molecules fall into the second category. In 1999, Vögtle and coworkers introduced a new threading method in which anion binding of a bulky phenolate (a stopper precursor) by a tetraamide macrocycle is used to assemble a complex termed a "wheeled nucleophile" or "semi-rotaxane" [12,13]. This complexed phenoxide anion reacts with a stoppered electrophile through the annulus of the macrocycle (making an axle inside the wheel) and thus a rotaxane is produced (Scheme 3.1) . Yields of up to a spectacular 95% have been obtained by this method, although more commonly yields are below 50%. The lack of any anion binding sites in the axle means that these rotaxanes were not designed as potential anion receptors.

One year later, this elegant anion recognition-directed threading methodology was employed by Smith and coworkers in the synthesis of ion-pair binding rotaxanes [14]. They used macrobicyclic wheels comprising a cation binding macrocycle bridged by an anion binding cleft (Scheme 3.2). The anion binding isophthalamide site played its major role during the synthesis of these systems using Vogtle's methodology, but was also shown to bind anions after the rotaxane assembly [15]. The cation binding crown ether macrocycle allowed for cation binding-induced modulation of the rotaxane's dynamics [16].

Further investigation of this template motif by Schalley and coworkers revealed certain limitations of this methodology, namely that application of less bulky phenolates gave disappointingly low yields of rotaxanes [17]. This was traced back to the double role of phenolate oxygen, which acts both as a nucleophile and the assembly-directing anionic agent at the same time. To circumvent this problem, they designed a modified thread in which the only role of the phenolate anion was to direct the assembly of the pseudorotaxane precursors (Scheme 3.3) [18]. This assembly is subsequently locked by covalent attachment of two stoppers, which occurs at amino groups remote from the recognition site. Interestingly, the phenolate anion encapsulated inside the rotaxane does not react even with very powerful alkylating agents such as methyl iodide.

Such protection of a thread by a macrocycle was also used by Smith and co-workers to stabilize near-infrared dyes, squaraines, in the form of rotaxanes (Scheme 3.4) [19]. These examples are also notable because of the role of anion recognition in their synthesis. More precisely, the macrocyclic wheel associates around the squaraine thread, which acts as a template by virtue of its negatively charged oxygen atoms.

The above examples leave no doubt that anion recognition may be used advantageously to direct the assembly of intertwined structures. However, in all of the above methods, negatively charged groups are covalently attached parts of the assembling structures and furthermore none of these methods have been extended to the synthesis of catenanes thus far. To uncover the full potential of anion templation in supramolecular synthesis, the use of discrete anions as interpenetrating templates needs to be developed in analogy with what has been achieved with cationic templates by Sauvage and others [20]. We set ourselves the challenge to achieve this goal.

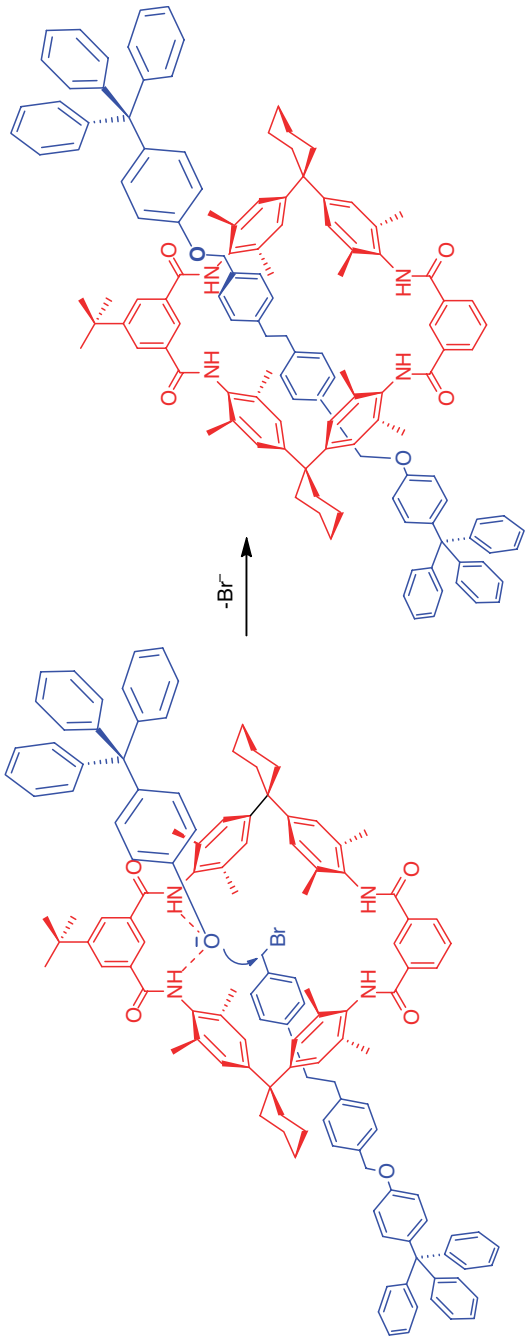

Scheme 3.1

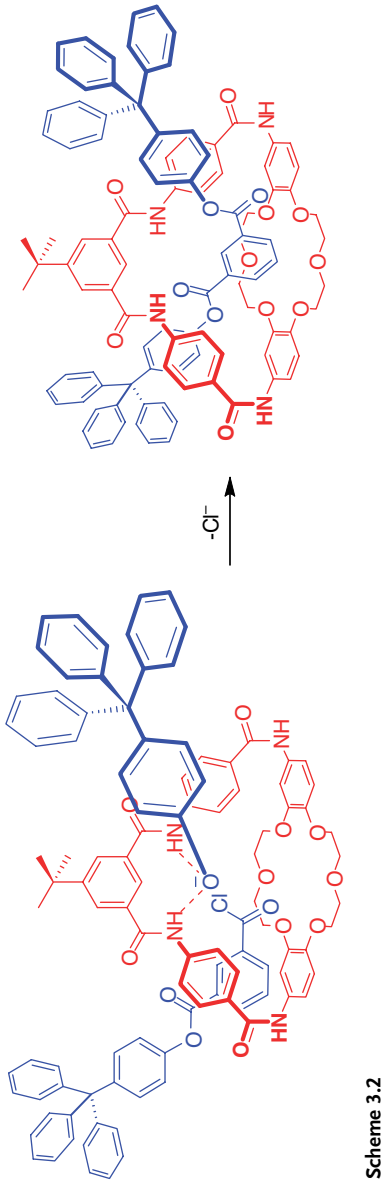

Scheme 3.2

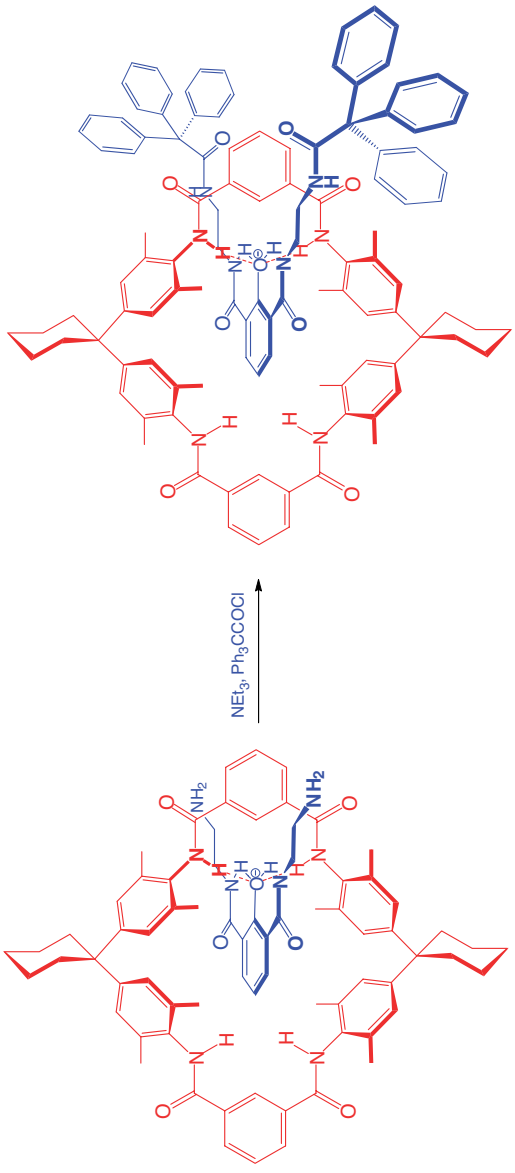

Scheme 3.3

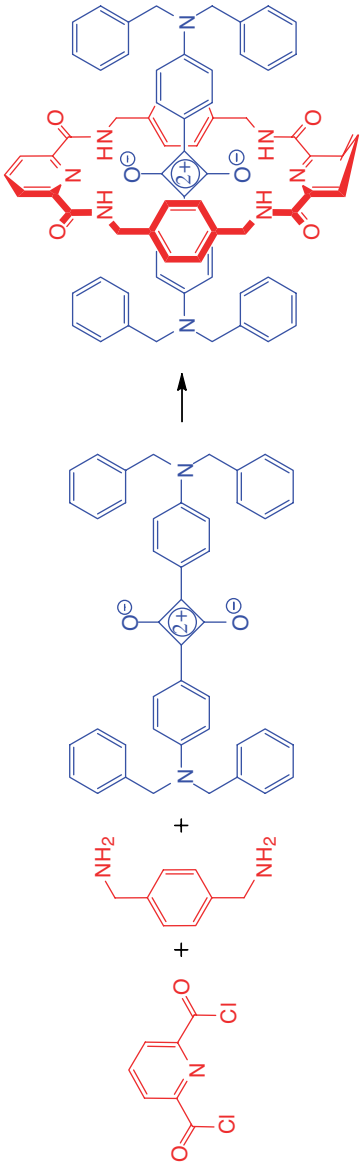

Scheme 3.4

3.3 Design of a General Anion Templation Motif

The basic motif in the cation templated syntheses of intertwined structures is an orthogonal assembly of two U-shaped ligands held together by a spherical metal cation. With the aim of producing an analogous motif but with reversed polarity, we focused on simple spherical halide anions.

A key requirement for an interwoven template is that it brings together two components and directs them in a more or less perpendicular manner. Of course, it is topology, not geometry, that matters here, so in principle any nonplanar arrangement should be equally good. However, from the practical point of view it is far more desirable that a perpendicular arrangement is formed, as it minimizes the probability of unwanted reactions such as macrocyclization. Sauvage achieved perpendicular arrangements of phenanthroline ligands using the copper(I) cation, which has a strong preference for tetrahedral coordination and this feature of the metal cation template was often mentioned as indispensable for the success of catenane synthesis. This calls into question the idea of using halide anions for the same purpose, as they have no marked geometric preferences and are therefore certainly unable to compel geometric relationships between organic building blocks in a manner close to that achieved by transition metal cations. However, the same effect can be achieved by steric repulsion between ligands, thus leaving only one requirement for the potential template – its ability to interact simultaneously with two or more ligands strongly enough to overcome the unfavorable entropy of association and mutual repulsions of ligands.

The simple isophthalamide cleft receptors introduced by Crabtree were deemed to be good analogs of phenanthroline ligands because they are planar, U-shaped and bind halide anions strongly in nonpolar organic solvents (Figure 3.2) [21]. Unfortunately, however, their halide complexes exhibit exclusive 1 : 1 stoichiometry. To overcome this problem, a new pyridinium-based ligand **2** was designed, in which a positive charge was introduced to the aromatic ring, while the anion binding site was left unaltered [22]. This new ligand exists as a tightly associated ion pair with halide counterions, with an association constant $K_{ass} > 10^5\,M^{-1}$ estimated for the equilibrium:

$$\mathbf{2}^+PF_6^- + TBA^+Cl^- \rightleftharpoons \mathbf{2}^+Cl^- + TBA^+PF_6^-$$

by ^1H NMR titration in acetone-d_6. The chloride anion is strongly held within the binding cleft of this receptor by a combination of electrostatic and hydrogen bonding interactions and importantly its coordination sphere is still unsaturated: the anion presents an empty meridian orthogonal to the pyridinium cation, which is available for further complexation to a second hydrogen bond donating ligand. This desired association indeed occurred and the isopthalamide compound **1** and pyridinium chloride ion pair $\mathbf{2}^+Cl^-$ produced a 1 : 1 association constant of $100\,M^{-1}$ in acetone-d_6, whereas no association was observed for weakly coordinating anions such as hexafluorophosphate (Figure 3.2).

It is worth noting, that under the conditions used, the above process is exclusively observed as heterodimerization. This is due to each pyridinium receptor associating

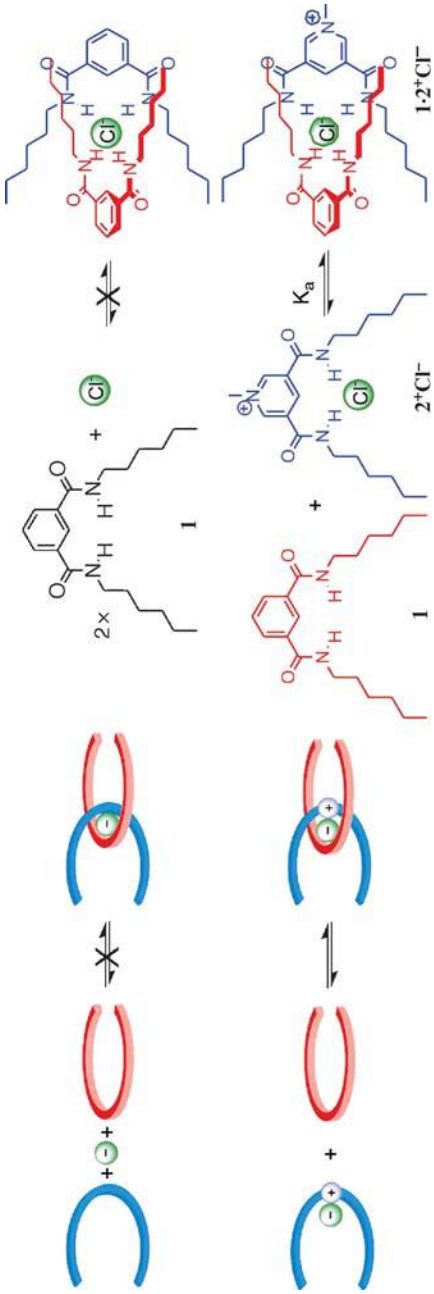

Figure 3.2 Anion-templated assembly of orthogonal complexes. In acetone-d_6, K_{ass} has a value of 100 M^{-1}.

strongly with its own chloride, so that the anions are not shared, whereas, as already discussed, the isophthalamide itself has no propensity for the formation of 2 : 1 complexes.

Encouraged by this result, we elaborated the second component of the self-assembly, isophthalamide cleft receptor in such a way so as to strengthen the heterodimeric complex by additional interactions (Figure 3.3) [23]. Thus the sequential introduction of an electron-rich hydroquinone moiety (**3**) and ether oxygens (**4**) led to incremental enhancements in the anion-templated orthogonal complex association constants, as measured by ^{1}H NMR titrations in dichloromethane-d_2. The hydroquinone functionality allows π-donor–π-acceptor interactions to occur with the pyridinium cation unit, with such interactions being detectable by UV/visible spectroscopy. The extra ether oxygens then form weak, charge-assisted C−H···O hydrogen bonds with the *N*-methyl group. However, these interactions are secondary to the anion templation event, as no orthogonal complex formation could be detected in the presence of noncoordinating anions, such as hexafluorophosphate.

3.4 Anion-templated Interpenetration

All the above structural elements were combined in the structure of the macrocyclic receptor **5**, designed to demonstrate anion-templated threading [22]. As was hoped, the chloride salt of pyridinium receptor $\mathbf{2}^+Cl^-$ threaded through the annulus of the macrocycle driven by the affinity of the halide anion for the isophthalamide cleft. This is evidenced by characteristic changes in ^{1}H NMR spectra of both components observed upon their mixing. First, large downfield shifts in the macrocycle isophthalyl and amide protons (C) are seen, indicative of anion binding within macrocycle's cleft. At the same time, upfield shifts in the pyridinium aromatic and amide protons (A) suggest loosened interactions between pyridinium cleft and anion. These two observations are consistent with both threading and competition between receptors for chloride binding, with the second explanation being disfavored by much stronger affinity of charged pyridinium receptor to the anion. The definite proof of threading comes from an upfield shift of the macrocycle hydroquinone proton signals (D) and aromatic C−H protons of the thread caused by π-stacking interactions. Additionally, weak hydrogen bonding interactions between the pyridinium *N*-methyl protons and the ether oxygen atoms are manifested by a small downfield shift of the methyl group signal (B) (Figure 3.4). Thus, ^{1}H NMR spectroscopy confirms the presence of all primary and secondary stabilizing interactions incorporated into our design.

Quantitative ^{1}H NMR titration experiments carried out in acetone-d_6 revealed that the strength of the pseudorotaxane assembly is critically dependent upon the nature of the templating anion. Thus, when chloride is the thread counterion, the pseudorotaxane has an association constant of 2400 M^{-1}, but for bromide, iodide and hexafluorophosphate the constants are lower, being 700, 65 and 35 M^{-1}, respectively. This reflects the relative complexation abilities of these anions.

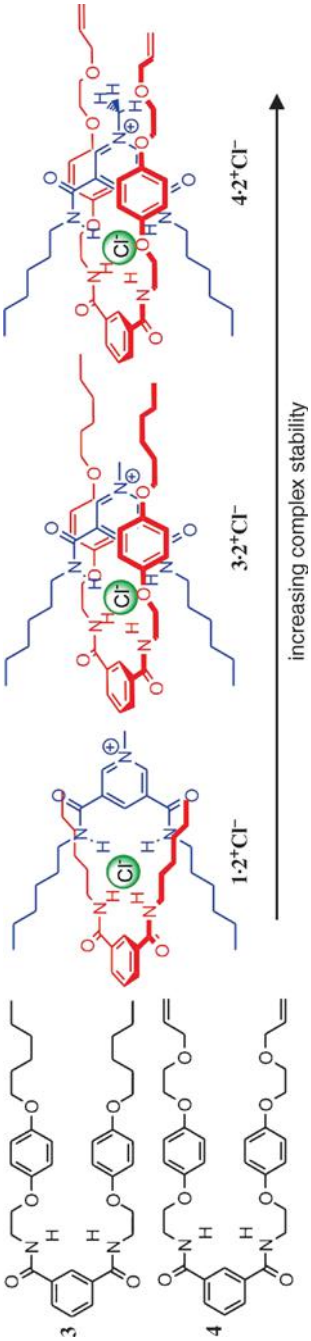

Figure 3.3 Increasing the strength of orthogonal complex formation using secondary interactions.

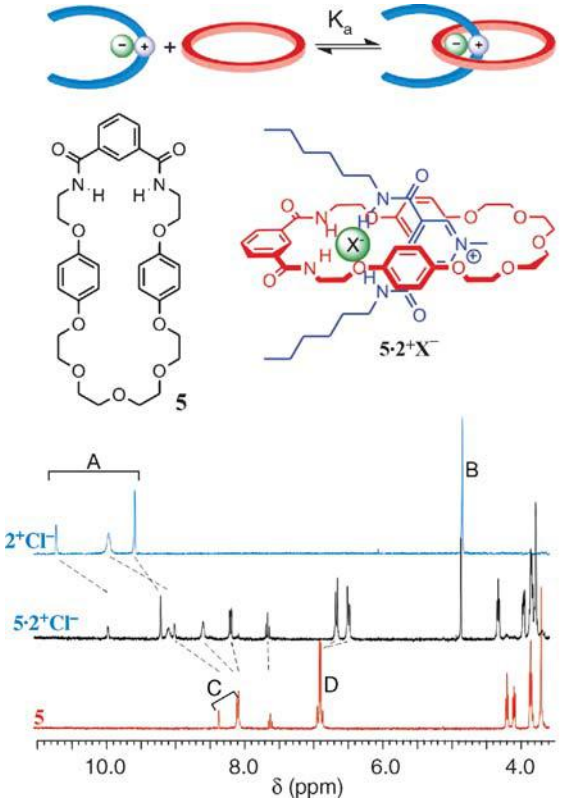

Figure 3.4 Formation of anion-templated [2]pseudorotaxane. General scheme (top), macrocycle **5** and pseudorotaxane $\mathbf{5{\cdot}2}^{+}Cl^{-}$ (middle) and ^{1}H NMR spectroscopic evidence for pseudorotaxane formation (bottom). For spectrum labeling, see text.

Single-crystal X-ray analysis further confirmed the interlocked nature of the assembly and the presence of all the secondary stabilizing interactions inferred from the ^{1}H NMR spectra (Figure 3.6). Furthermore, it gives a detailed picture of the anion binding cavity. The amide hydrogen bond donors are shown to form an approximately tetrahedral coordination sphere around the spherical chloride anion, resulting from an orthogonal arrangement of the organic components. Additionally, the anion forms two short C–H···Cl hydrogen bonds, one with each aromatic ring.

3.5
Probing the Scope of the New Methodology

The large amount of detail required in the design of the first anion-templated pseudorotaxane provoked a question about the versatility of this templation strategy.

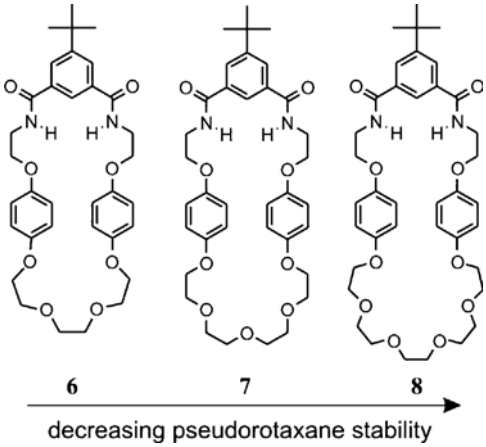

Figure 3.5 Variation of [2]pseudorotaxane stability with macrocycle ring size.

To address this question, we independently varied (i) the structure of the macrocycle, (ii) the thread and (iii) the nature of the anion [24].

The length of the macrocyclic polyether chain was found to affect significantly the stability of the [2]pseudorotaxane assemblies with the pyridinium chloride thread, which decreased with increasing ring size: **6** > **7** > **8** (Figures 3.5 and 3.6). As the anion binding ability of the macrocycles remains unaltered in this series, this trend was explained in terms of increasing entropic cost of association resulting from the increasing flexibility of the polyether chains and decreasing second-sphere stabilization between complexes.

ITC investigations on **6**·**2**$^{+}$Cl^{-} and **7**·**2**$^{+}$Cl^{-} in 1,2-dichloroethane revealed that although in both cases the association was enthalpy driven and opposed by entropy, the entropic cost of association was much higher for **7**·**2**$^{+}$Cl^{-} than for **6**·**2**$^{+}$Cl^{-}.

Subtle differences in second sphere stabilization were found in the X-ray structures of pseudorotaxanes **6**·**2**$^{+}$Cl^{-}, **5**·**2**$^{+}$Cl^{-} (which differs from **7**·**2**$^{+}$Cl^{-} with *t*-Bu group only) and **8**·**2**$^{+}$Cl^{-} (Figure 3.6). The smallest macrocycle **6**·**2**$^{+}$Cl^{-} is apparently

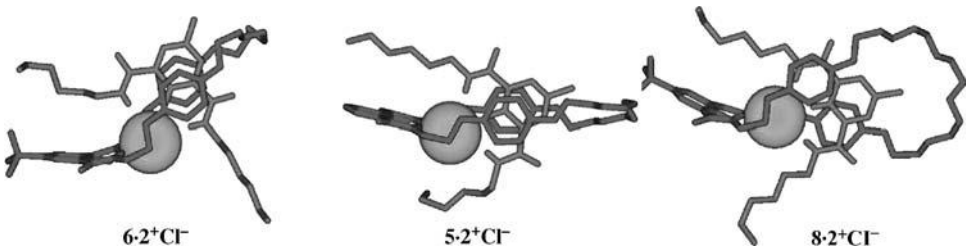

Figure 3.6 Single-crystal X-ray structures of [2]pseudorotaxanes **6**·**2**$^{+}$Cl^{-}, **5**·**2**$^{+}$Cl^{-} and **8**·**2**$^{+}$Cl^{-}. All hydrogens except those in the primary anion coordination sphere have been omitted for clarity. Chloride is represented as a space-filling sphere.

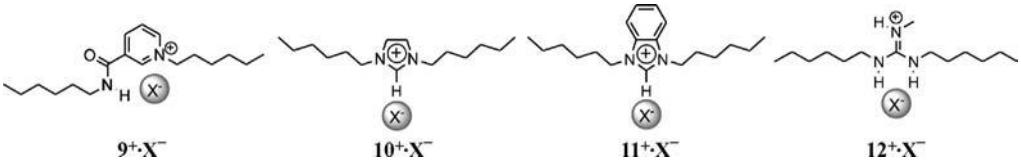

Figure 3.7 Alternative threads for pseudorotaxane assembly.

too small to encircle the thread and, as a result, the pyridinium ring of the thread lies out of the plane of the polyether ring. This allows for a short bifurcated hydrogen bond between the aromatic CH proton from the position 2 of the pyridinium ring and two ether oxygen atoms, which is not present in the crystal structures of the other two pseudorotaxanes. Another interesting feature was found in the crystal structure of the largest macrocycle **8**·**2**$^{+}$Cl^{-}. The π-stacking interaction between the pyridinium cation and one of the hydroquinones is greatly diminished in this complex, with the distance between ring centroids being 4.266 Å, versus 3.540–3.728 Å in other two cases. This observation suggests that **8** is too large to accommodate the pyridinium chloride ion pair comfortably.

The above structure–affinity investigations were subsequently extended to other types of cationic threads based on the nicotinamide, imidazolium, benzimidazolium and guanidinium moieties (Figure 3.7) [25]. All these threads, as chloride salts, form interpenetrated complexes with macrocyclic receptors **6–8**, illustrating the versatility of this anion templating methodology. However, the stability of these complexes was lower and decreased across the above series, as a result of the decreasing role of second-sphere coordination effects. This is not surprising given that these macrocycles were deliberately optimized for *N*-methylpyridinium-based threads. As a corollary, a much less pronounced effect of macrocycle size on pseudorotaxane stability was observed in these cases (Figure 3.8).

The key role of anion binding in all the above assembly processes is evidenced by the observation that the stability of pseudorotaxanes increases with the hydrogen bond accepting ability of anions in the series $PF_6^- < I^- < Br^- < Cl^-$ [7].

Thus the stability of the resulting pseudorotaxane systems is heavily dependent on the nature of the components, in particular the nature of the templating anion, but also on the size of macrocycle, propensities for secondary stabilizing interactions and

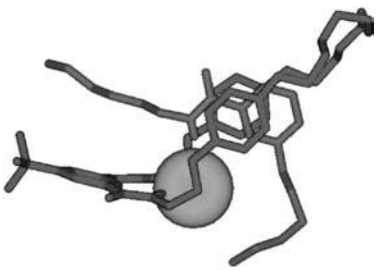

Figure 3.8 Single-crystal X-ray structure of **7**·**9**$^{+}$Cl^{-}.

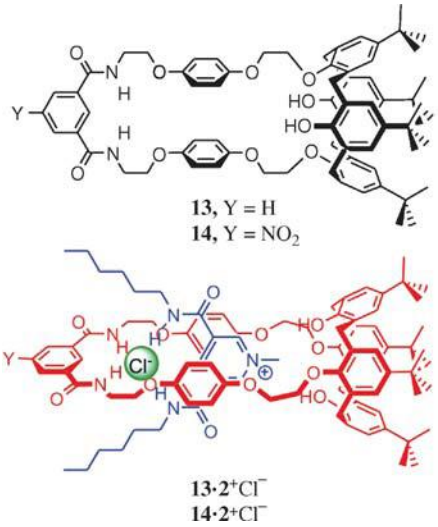

Figure 3.9 Calix[4]arene macrocycles for [2]pseudorotaxane formation.

the strength of thread-anion pairing. Importantly, however, in the presence of chloride anion all the above cationic threads do form pseudorotaxanes, demonstrating structural versatility of the methodology. This encouraged us to divert even further from the original design of macrocycle.

First, the crown ether portion of **6**–**8** was replaced with a calix[4]arene unit, as in **13** (Figure 3.9) [26]. This macrobicycle also undergoes [2]pseudorotaxane formation on treatment with thread $\mathbf{2}^{+}Cl^{-}$, although the association constant is much reduced ($170\ M^{-1}$ in acetone-d_6) compared with the simpler systems, possibly due to steric constraints. It is possible to enhance pseudorotaxane stability by improving the anion binding properties of the macrocycle. Thus the introduction of a 5-nitro group into isophthalamide moiety (as in **14**), which increases the hydrogen bond acidity of the amide donors, also increases the observed pseudorotaxane association constant ($240\ M^{-1}$ in acetone-d_6).

Second, the anion binding isophthalamide fragment of the macrocycle was exchanged for rhenium(I) bipyridylbisamide unit, which may be thought of as an expanded version of isophthalamide moiety with two aromatic CH hydrogen bond donors instead of just one (Figure 3.10) [27].

Its major advantage is the potential to provide an optical signal for anion binding [28] and, when the anion is paired to a suitable thread, for pseudorotaxane formation. Macrocycle **15** was shown by ^{1}H NMR titrations in acetone-d_6 to bind anions much more strongly than isophthalamide macrocycles and, accordingly, formed strong, interpenetrated complexes with the halide salts of pyridiniumdiamide, pyridinium-nicotinamide, benzimidazolium and guanidinium cations in the same solvent. The single-crystal X-ray structure determination of the macrocycle-pyridinium chloride complex (Figure 3.11) shows the interpenetrated nature of the assembly and binding

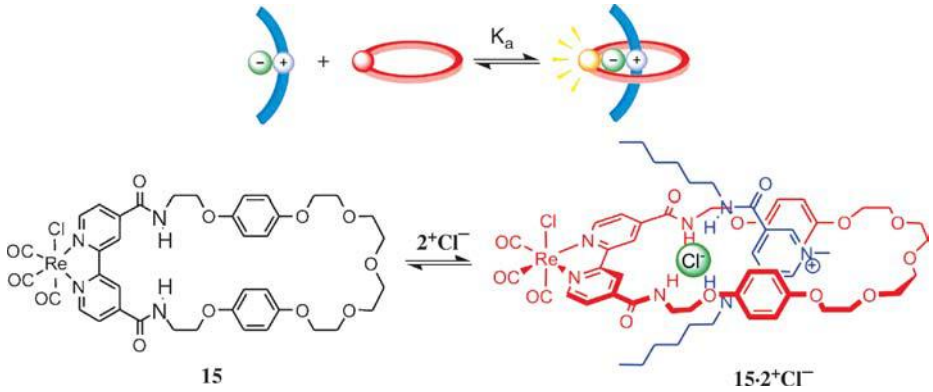

Figure 3.10 Luminescence sensing of [2]pseudorotaxane assembly using a rhenium-containing macrocycle. General schematic (top) and formation of pseudorotaxane **15**·**2**$^{+}$Cl^{-} (bottom).

of the chloride anion by seven hydrogen bonds: four with amide NH protons, two with 3,3′-bipyridyl CH protons and one with 4-pyridinium CH proton. Interestingly, it is the only crystal structure available thus far in which hydroquinone rings and pyridinium ring are not offset but lie directly one above the other. This is probably simple geometric consequence of larger bite size of bipyridyl moiety in comparison to isophthalamide.

As was hoped, the addition of **2**$^{+}$Cl^{-} to the macrocycle was signaled through an enhancement in the rhenium–bipyridine ^{3}MLCT emissive response. This was exploited for anion sensing in a permanently locked system described later.

The successful formation of such a variety of pseudorotaxanes using anion templation demonstrated structural robustness of this methodology and encouraged its application in the synthesis of permanently interlocked derivatives.

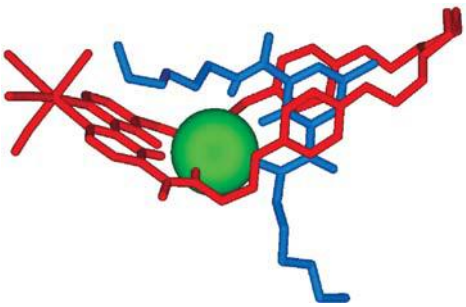

Figure 3.11 Single-crystal X-ray structure of **15**·**2**$^{+}$Cl^{-}. All hydrogens except those in the primary anion coordination sphere have been omitted for clarity. Chloride is represented as a space-filling sphere.

3.6
Anion-templated Synthesis of Rotaxanes

Having demonstrated the feasibility of using anions to direct the assembly of orthogonal complexes and pseudorotaxanes, it was hoped that the same methodology would be readily applicable to the synthesis of permanently interlocked rotaxane and catenane species. However, as mentioned above, discrete anionic templates have never been used for this purpose before and some practical problems were encountered on the way to this goal. One of them was the limited availability of suitably large stoppering groups. An inherent feature of our methodology is that a macrocycle has to be large enough to accommodate both thread and anion. As a corollary, we needed particularly bulky stoppers to prevent the macrocycle from slipping off. No such suitable building blocks are commercially available and an assortment of easy to make synthons in the literature is very restricted. Initially, the well-known amino-functionalized tetraphenylmethane-type stoppers appended with *tert*-butyl groups for added bulkiness were used.

Second, our choice of synthetic reactions was limited by the requirement of their compatibility with anion recognition. For example, reactions involving anions as substrates (nucleophiles) or products (nucleofuges) should be avoided in view of possible competition with the template. Furthermore, reactions taking place in nonpolar solvents are preferred, because such conditions maximize the strength of anion binding.

The above considerations made the "stoppering" route to rotaxanes problematic and prompted us to switch to a "clipping" methodology (Figure 3.12). This was achieved using a ring-closing olefin metathesis reaction, which is well known to give high yields in macrocyclizations, works very well in nonpolar solvents and has excellent functional group tolerability (depending on the catalyst) [20,29].

In a first system, two tetraphenyl stoppers were covalently attached to a pyridinium chloride threading unit making up a thread component $\mathbf{16}^{+}Cl^{-}$ (Figure 3.12). The second component was the above-described charge neutral macrocycle precursor **4**, terminating with allyl groups capable of undergoing ring-closing metathesis reaction. By virtue of the chloride anion template the two components associate strongly in non-competitive solvents and RCM reaction with Grubbs' catalyst in dichloromethane led to the expected [2]rotaxane product $\mathbf{17}^{+}Cl^{-}$ in 47% yield [23]. No rotaxane formation was detected with analogous bromide, iodide and hexafluorophosphate pyridinium salts, indicating the critical templating role of the chloride anion. It is noteworthy that in this case the second-sphere coordination interactions which support the primary chloride recognition process also facilitate the ring closure process around the ion pair thread by directing the allyl-terminated arms into close proximity.

Single-crystal X-ray structural analysis confirmed the interpenetrated nature of the product and gave valuable insight into the binding mode of the anion inside the rotaxane cavity (Figure 3.13). It turned out that the two stoppers are not just innocent spectators of the anion binding, but actually donate two C—H···Cl hydrogen bonds from phenyl rings adjacent to amide groups. Thus, the anion binding cleft of the

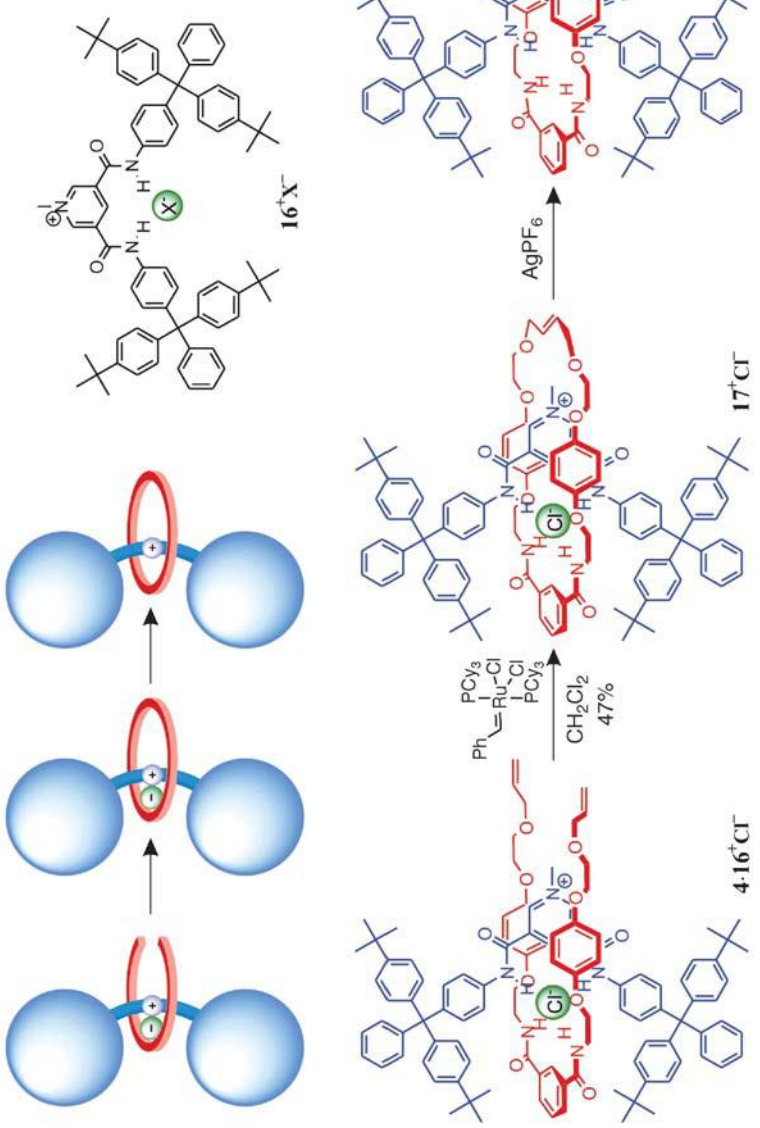

Figure 3.12 Formation of [2]rotaxanes. General scheme (top left), stoppered thread $\mathbf{16}^{+}Cl^{-}$ (top right) and formation of rotaxanes $\mathbf{17}^{+}Cl^{-}$ and $\mathbf{17}^{+}PF_6^{-}$ (bottom).

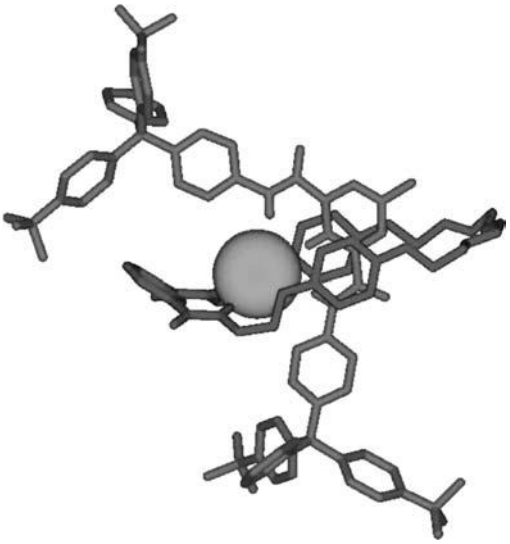

Figure 3.13 Single-crystal X-ray structure of $\mathbf{17}^{+}Cl^{-}$. All hydrogens except those in the primary anion coordination sphere have been omitted for clarity. Chloride is represented as a space-filling sphere.

thread is defined by five, not three, almost exactly coplanar hydrogen atoms. The anion's meridian is occupied by the macrocycle's isophthalamide cleft, which donates two strong hydrogen bonds from the amide groups. The third potential hydrogen bond donor, the internal aromatic proton of the isophthalamide unit, forms only a very weak bond with the anion, so that the coordination number of chloride in this complex may be thought of as seven. The structure also provides evidence for the existence of the second sphere π-stacking and $N^{+}-CH_3\cdots O$ hydrogen bonding interactions "designed into" this system.

Anion exchange of the chloride template for the noncoordinating hexafluorophosphate anion allowed us, for the first time, to compare the anion binding properties of the free and interlocked components. Satisfyingly, the [2]rotaxane $\mathbf{17}^{+}PF_6^{-}$ binds anions strongly in very competitive protic solvent mixture such as CH_3OH : $CDCl_3 = 1:1$ with remarkable reversal of selectivity with respect to the pyridinium thread (the macrocycle itself does not bind anions in this solvent system). Thus, whereas the thread binds anions according to their hydrogen bond accepting ability [$K_{(Cl^-)} = 125\ M^{-1}$, $K_{(H_2PO_4^-)} = 260$, $K_{11(AcO^-)} = 22\,000\ M^{-1}$, $K_{12(AcO^-)} = 140\ M^{-1}$), the rotaxane has a notable preference for chloride ($K = 1130\ M^{-1}$) over dihydrogenphosphate ($K = 300\ M^{-1}$) and acetate ($K_{11} = 100\ M^{-1}$, $K_{12} = 40\ M^{-1}$). This is postulated to be the result of a unique hydrogen bonding pocket of the rotaxane, formed by orthogonal clefts of the thread and macrocycle and its high degree of complementarity to the guest chloride anion. The complexation of larger anions would result in the significant, unfavorable distortion of the binding cavity thus reducing complex stability.

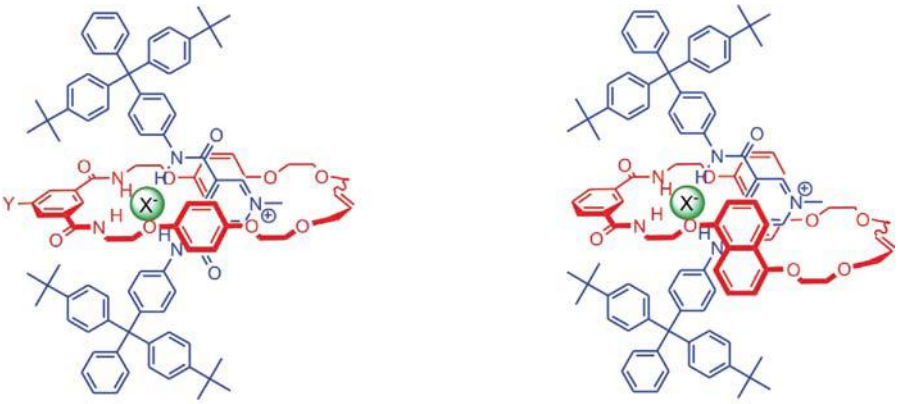

18^{+}Cl^{-}, Y=I, (43%)
19^{+}Cl^{-}, Y=NO_2, (60%)

20^{+}Cl^{-}, (15%)

Figure 3.14 Anion-templated [2]rotaxanes. The percentages in parentheses correspond to the yields of the [2]rotaxane formation step from the acyclic precursors.

This synthetic route to [2]rotaxanes has been used to generate a number of species similar to **17** (Figure 3.14) [30]. Again, the process is highly dependent on the nature of the templating anion and, interestingly, on the anion binding properties of macrocycle. The rotaxane yield was increased to 60% for the nitro-substituted rotaxane **19**, as a result of the precursor orthogonal complex assembly being more stable owing to increased amide hydrogen bond acidity. The structural tolerance of the method towards changes in the macrocycle structure was demonstrated by the synthesis of naphthyl-containing [2]rotaxane **20**. The yield was lower in this case (15%), perhaps due to the increase in macrocycle size and flexibility. Importantly, the interlocked nature of these systems could withstand the removal of the chloride anion template, which allowed the study of their anion binding properties. The introduction of the electron withdrawing nitro or iodo functionalities (**19**$^{+}PF_6^{-}$ and **18**$^{+}PF_6^{-}$) leads to an enhancement in anion binding, which was mirrored in the corresponding macrocycles. These results indicate that it is possible to fine tune the binding properties of the interlocked species by small structural changes of their components.

3.7
Anion-templated Synthesis of Catenanes

In a major development of this methodology, the first example of the use of anion templation in the synthesis of catenanes was demonstrated [31]. The strategy employed is shown in Figure 3.15. A chloride anion, as a part of tight ion pair, promotes the initial formation of a [2]pseudorotaxane and a subsequent clipping reaction afforded the [2]catenane structure.

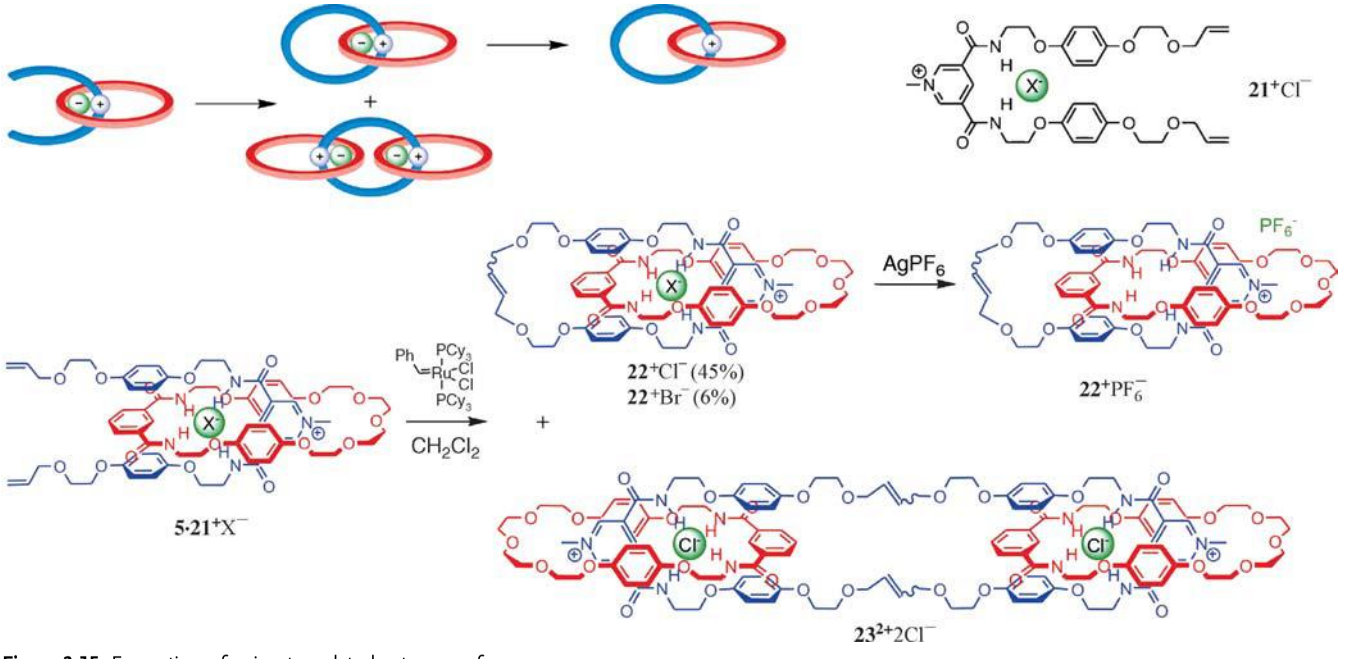

Figure 3.15 Formation of anion-templated catenanes from [2]pseudorotaxane precursor. General scheme (top left), structure of thread precursor **21** (top right) and formation of [2]-catenane **22** and [3]-catenane **23** (bottom). Yields for the catenane formation process are given in parentheses.

Mixing macrocycle **5** and pyridinium chloride allyl functionalized derivative $\mathbf{21}^{+}Cl^{-}$ in dichloromethane followed by addition of Grubbs' catalyst afforded the [2]catanene $\mathbf{22}^{+}Cl^{-}$ in 45% yield and a [3]catenane, $\mathbf{23}^{2+}2Cl^{-}$, in <5% yield (Figure 3.15). It is noteworthy that analogous RCM reactions of macrocycle **5** with the corresponding bromide pyridinium component gave the desired [2]catenane $\mathbf{22}^{+}Br^{-}$ in only 6% yield and no catenanes were isolated from RCM reactions of the macrocycle with iodide or hexafluorophosphate pyridinium derivatives. As with the [2]rotaxane synthesis discussed previously, this again highlights the crucial role the chloride ion template plays whereby threading of the pyridinium cation $\mathbf{21}^{+}$ is driven by recognition of its chloride counterion by the macrocycle.

The interlocked nature of the product was established both from NMR spectroscopic experiments and single-crystal X-ray analysis (Figure 3.16). It was clear from this structure that chloride is essential in controlling the orientation of the two interpenetrated components and that the secondary π-stacking and hydrogen bonding interactions involving the pyridinium function are present. The anion is held within the catenane cavity by six hydrogen bonds, four with amide groups and two with aromatic protons located between amide arms. The pyridinium cation is sandwiched between two hydroquinone rings, whereas the isophthalamide moiety forms a less perfect stacking with just one hydroquinone moiety.

The removal of the chloride anion template was achieved by addition of silver hexafluorophosphate to produce the [2]catenane$^{+}PF_6^{-}$ salt. Quantitative ^{1}H NMR binding studies in methanol-d_4:chloroform-d_3 1 : 1 mixture revealed that the pyridinium macrocyclic precursor $\mathbf{21}^{+}PF_6^{-}$ displays a strong affinity for acetate and dihydrogen phosphate and only binds chloride weakly, whereas the catenane $\mathbf{22}^{+}PF_6^{-}$ exhibits a reverse binding trend: $Cl^{-} > H_2PO_4^{-} > AcO^{-}$. Table 3.1 shows that chloride anion binding is significantly enhanced upon catenane formation, whereas the binding of the oxoanions is weakened. In a similar fashion to the [2]rotaxane binding studies discussed previously, the removal of the templating anion creates a unique topologically defined hydrogen bond donating pocket which is highly selective for chloride anions.

Furthermore, the assembly process is tolerant of major changes in the neutral macrocyclic components, with for example the [2]catenane $\mathbf{24}^{+}Cl^{-}$ being formed in 29% yield from reaction of calix[4]arene macrocycle **13** and $\mathbf{21}^{+}Cl^{-}$ (Figure 3.17) [17].

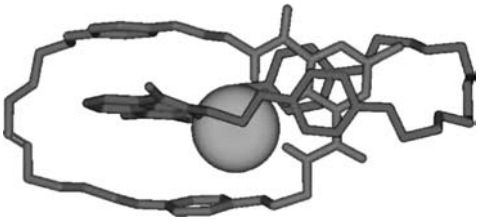

Figure 3.16 Single-crystal X-ray structure of $\mathbf{22}^{+}Cl^{-}$. All hydrogens except those in the primary anion coordination sphere have been omitted for clarity. Chloride is represented as a space-filling sphere.

Table 3.1 Comparison of anion binding properties of macrocycle precursor **21**$^{+}PF_6^{-}$ and catenane **22**$^{+}PF_6^{-}$. Units M^{-1}, solvent 1 : 1 $CD_3OD-CDCl_3$, errors <10%.

	Cl^-	$H_2PO_4^-$	AcO^-
21$^{+}PF_6^{-}$	$K_{11} = 230$	$K_{11} = 1360$ $K_{12} = 370$	$K_{11} = 1500$ $K_{12} = 345$
22$^{+}PF_6^{-}$	$K_{11} = 730$	$K_{11} = 480$ $K_{12} = 520$	$K_{11} = 230$

As before, this process was reliant on the presence of a suitable anion template and exchange of this template to give the hexafluorophosphate salt **24**$^{+}PF_6^{-}$ also proved possible.

As mentioned in the Introduction, the development of our anion templation methodology was inspired by Sauvage's elegant synthesis of a [2]catenane by two simultaneous macrocyclizations performed on an orthogonal precursor complex assembled around a copper(I) cation. Thus, the ultimate challenge for our newly developed methodology was to emulate this "double clipping" synthesis. This has recently been achieved with the assembly of two identical acyclic pyridinium precursors around a single chloride anion template followed by a double ring closing metathesis reaction, which yielded the doubly charged catenane **26** in excellent yield (Figure 3.18) [32].

In this experiment, a pyridinium-based macrocyclic precursor **25**$^{+}X^{-}$, featuring extended polyether chains, was used. Addition of TBA$^{+}Cl^{-}$ to **25**$^{+}PF_6^{-}$ in $CDCl_3$ led to the observation by ^1H NMR spectroscopy of the coexistence of 1 : 1 and 1 : 2 host–guest complexes, indicating the presence of an interwoven assembled species. Further evidence of the orthogonal assembly was provided by the upfield shifts of the hydroquinone protons, due to the familiar effect of favorable π–π stacking interactions. Mixing an equimolar solution of **25**$^{+}Cl^{-}$ and **25**$^{+}PF_6^{-}$ in dichloromethane, followed by double macrocyclization using Grubbs' catalyst, afforded the dicationic [2]catenane **26** in the exceptionally high yield of 78% (Figure 3.18). When the hexafluorophosphate salt **25**$^{+}PF_6^{-}$ was so treated, the [2]catenane product **26**$^{2+}2PF_6^{-}$ also formed, but in much lower yield (16%). This demonstrates the role of secondary interactions which, in the absence of chloride template and with

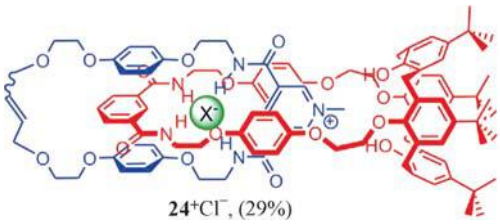

24$^{+}Cl^{-}$, (29%)

Figure 3.17 Calix[4]arene catenane **24**.

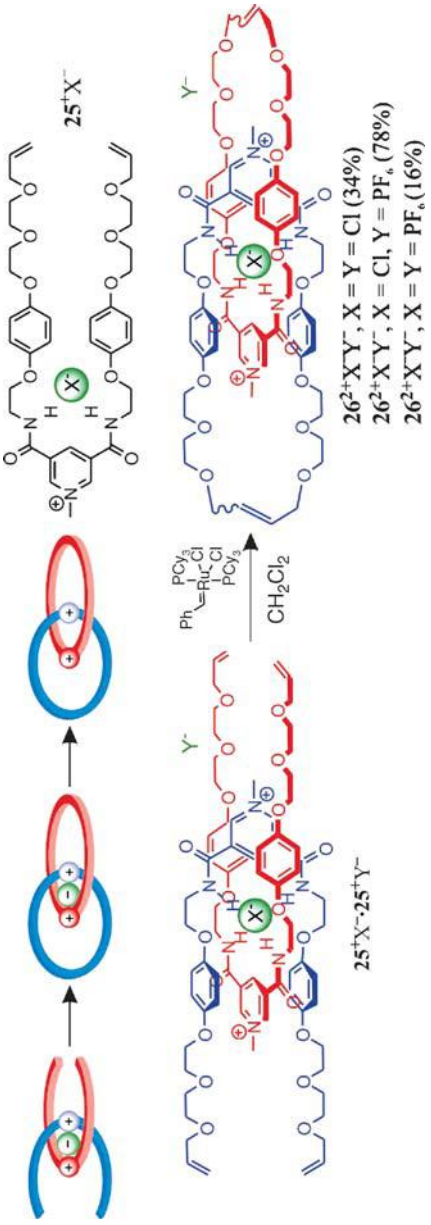

Figure 3.18 "Double clipping" route to [2]catenane. General schematic (top left), precursor molecule **25** (top right) and formation of [2]catenanes **26** (bottom).

possible aid from weak hexafluorophosphate binding, direct the assembly of the orthogonal complex. Of course, the presence of a templating chloride anion substantially enhances the efficacy of the reaction. The 2 : 1 receptor : template ratio is essential; when the chloride precursor $\mathbf{25}^{+}Cl^{-}$ was treated with Grubbs' catalyst, the yield of catenane product was lower (34%) due to competition from 1 : 1 binding mode, which favors simple macrocyclization.

Single-crystal X-ray structural analysis of $\mathbf{26}^{2+}Cl^{-}PF_6^{-}$ confirms the interlocked nature of the product and reveals its self-complementary structure – the two macrocycles bind each other more efficiently than in the previous unsymmetrical catenane due to the presence of a second, positively charged, pyridinium ring instead of neutral isophthalamide moiety. This permits stronger π-stacking interactions, additional hydrogen bonding with ether oxygens and also strengthens anion binding. These effects explain the extraordinarily high yield obtained in this synthesis (even without optimization).

There is an excellent match between the guest chloride anion and the host cavity. The anion is coordinated by six hydrogen bonds in a distorted octahedral manner and, as shown by space-filling model, almost completely surrounded by the catenane molecule (Figure 3.19).

Anion exchange with $AgPF_6$ gave $\mathbf{26}^{2+}2PF_6^{-}$ whose anion binding properties were investigated by ^{1}H NMR spectroscopic titration in $CDCl_3$–acetone-d_6 (1 : 1). Analysis of the titration data obtained upon the addition of chloride, bromide and acetate produced association constants with a major 1 : 1 host:guest binding stoichiometry and a minor 1 : 2 binding component. The association constants reveal a remarkable selectivity for chloride ($K_{11} = 9240\ M^{-1}$, $K_{12} = 160\ M^{-1}$) over bromide ($K_{11} = 790\ M^{-1}$, $K_{12} = 40\ M^{-1}$) and acetate ($K_{11} = 420\ M^{-1}$, $K_{12} = 40\ M^{-1}$).

It is noteworthy that this "double clipping" catenane synthesis is much shorter than the previous one, owing to the symmetrical structure of the product; the two wheels in previous catenane, although very similar, required independent synthesis. More generally, it is a great advantage of catenanes over rotaxanes that the sometimes laborious synthesis of stoppers and threads is no longer required. This advantage grows in importance with the increasing size of wheels, which requires larger and larger stoppers.

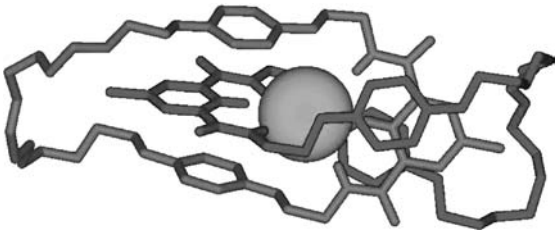

Figure 3.19 Single-crystal X-ray structure of $\mathbf{26}^{+}Cl^{-}PF_6^{-}$. All hydrogens except those in the primary anion coordination sphere have been omitted for clarity. Chloride is represented as a space-filling sphere.

3.8
Functional Properties of Anion-templated Interlocked Systems

Thus far it has been shown that the unique interlocked binding domain topology lends anion-templated rotaxanes and catenanes interesting anion binding characteristics distinct from their "parent" species. The observed increase in binding strength coupled with reversal of selectivity makes these interlocked structures of great interest in the molecular sensing arena. In order to apply these receptors to anion sensing, it is necessary to provide some means of signal transduction and amplification. The above-described advances in templation methodology have made the synthesis of such sophisticated structures, equipped with reporter groups able to signal the recognition event by electrochemical or spectroscopic means, possible. Another challenge on the way to practical applications is the attachment of molecular sensors to a solid surface, which is a prerequisite for robust device fabrication. Recent progress towards these goals is outlined below.

The first photo-active anion-sensing rotaxane was based on a luminescent rhenium(I) bipyridyl motif being incorporated into macrocyclic wheel (Figure 3.20), as in the previously described pseudorotaxane $\mathbf{15}\cdot\mathbf{2}^{+}Cl^{-}$ [33]. The chloride derivative $\mathbf{27}^{+}Cl^{-}$ was prepared in 21% yield via the now established ring clipping of the neutral rhenium(I) bipyridyl-containing precursor **29** around the pyridinium chloride thread $\mathbf{28}^{+}Cl^{-}$; the bulky calix[4]arene stopper groups were necessary to prevent dethreading of the larger macrocycle. As before, replacement of the chloride template with hexafluorophosphate gave a [2]rotaxane $\mathbf{27}^{+}PF_6^{-}$ which contained not only a three-dimensional anion binding domain but also a luminescent transition metal bipyridyl center able to sense optically the anion binding event. Thus the addition of TBA anion salts to a solution of $\mathbf{27}^{+}PF_6^{-}$ in acetone induced an enhancement in the ^{3}MLCT emission band intensity of the rotaxane receptor. Titration experiments in acetone demonstrated that the rotaxane selectively bound hydrogensulfate ($K_a > 10^6\,M^{-1}$) over nitrate and chloride, which contrasts with the properties of the macrocycle **30**, which was selective for chloride ($K_a = 8.7 \times 10^4\,M^{-1}$). Receptors selective for hydrogensulfate are rare, because hydrogensulfate anion is a poor hydrogen bond acceptor. Importantly, an anion templation approach may therefore be used to synthesize molecular sensors for anions different from template.

The above rotaxane sensor utilizes a common sensing mechanism based on electronic communication between anion and reporter group. However, rotaxane- and catenane-based receptors offer some potential means of signal transduction that are unique to interlocked structures, based on the mutual relationships between the mechanically bound subunits. For example, anion binding may amplify/reduce the interactions between thread and macrocycle and, as a consequence, alter spectroscopic or electrochemical properties of the rotaxane. Alternatively, anions may induce co-conformational change, such as shuttling of the macrocycle along the thread, which could also translate into an observable signal. Although basic mechanisms underlying the signal generation in the above examples are well developed and routinely used to study, for example, molecular switches or machine-like behavior of interlocked molecules, their application to molecular

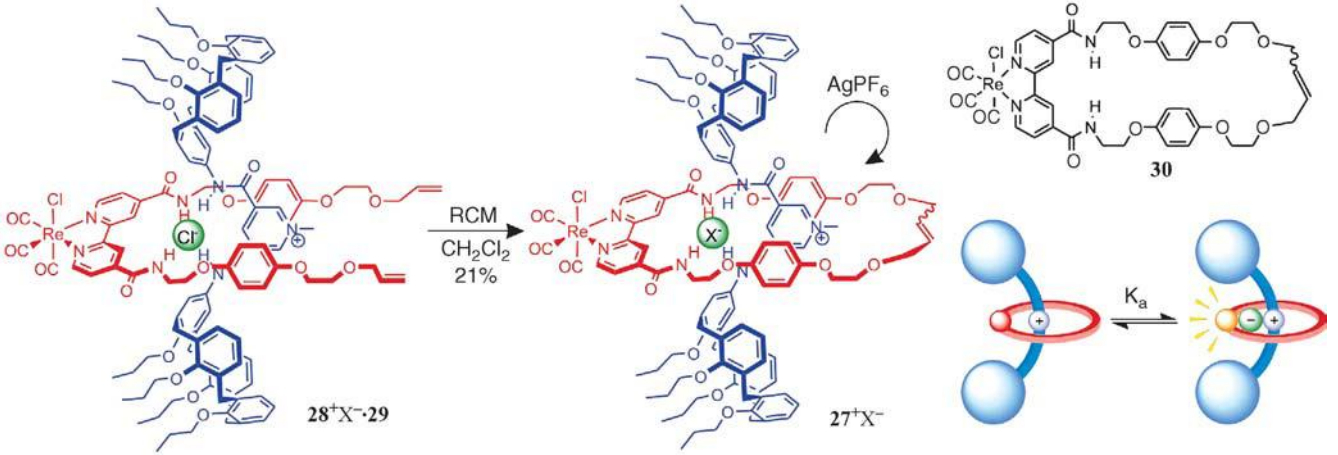

Figure 3.20 [2]Rotaxane anion sensor. Formation of luminescent rotaxanes $\mathbf{27}^+Cl^-$ and $\mathbf{27}^+PF_6^-$ from the precursors $\mathbf{28}^+Cl^-$ and **29** by anion-templated Grubbs' ring closing metathesis (left), luminescent macrocycle **30** (top right) and schematic for rotaxane anion sensing (bottom right).

sensing is underexplored, due to the lack of guest binding cavities in previously described catenanes and rotaxanes.

As a prototype sensing system illustrating this paradigm, we set about constructing a pseudorotaxane system with a through-space communication between thread and macrocycle components, which may be influenced by anion binding. The mechanism used to accomplish this was photoinduced energy transfer between a rhenium (I) bipyridyl sensitizer incorporated within the macrocycle **31** and a luminescent lanthanide complex appended to one terminus of the benzimidazolium threads **32** (Figure 3.21) [34]. Addition of threads containing no lanthanide center, or a lanthanide center not suitable for energy transfer such as gadolinium (**32a**), to the rhenium macrocycle **31** resulted in an enhancement of ^{3}MLCT luminescent emission, as observed in **15** and **27**$^+PF_6^-$ above. For threads containing a suitable lanthanide metal such as neodymium or ytterbium, however, no such enhancement was observed on pseudorotaxane formation; indeed, for the neodymium thread **32c** a significant quenching of the rhenium-centered luminescence was observed. Furthermore, the evolution of new near-infrared (NIR) emission bands consistent with lanthanide metal emission could be detected. This observation is consistent with the proposed energy transfer between the ^{3}MLCT excited state of the rhenium(I) bipyridyl center and the lanthanide complex. As such an energy transfer process is highly dependent on the distance between the two metal centers, the appearance of NIR luminescence indicates the proximity between the stopper and macrocycle and hence pseudorotaxane formation, which is in turn anion dependent. Thus the same principle may be used for anion sensing or, for example, to monitor anion-induced shuttling of the macrocycle along the thread in a prototype molecular machine-like device based on an anion recognition process.

The confinement of interlocked anion receptors at electrode surfaces should allow the harnessing of their specific binding behavior in electrochemical sensing materials. This possibility was probed by the formation of self-assembled monolayers (SAMs) of redox-active bis-ferrocene functionalized pseudorotaxane **33**·**34**$^+Cl^-$ at a gold surface; the transformation results in a rotaxane with the gold electrode effectively acting as a stopper (Figure 3.22) [35]. The presence of two different redox-active centers on the thread and on the macrocycle allowed for independent monitoring of their presence on the electrode surface. The replacement of the chloride template with hexafluorophosphate proved possible without disrupting the interlocked nature of the surface assembled rotaxanes. The anion binding properties of this redox-active rotaxane-SAM could be probed using electrochemical methods, examining the perturbations in the two redox waves of the system on the addition of various analytes; proximal anion binding should be accompanied by a cathodic shift due to electrostatic stabilization of the oxidized ferrocene unit. In acetonitrile solutions the ferrocene unit of the rotaxane macrocycle was shown to demonstrate a selective voltammetric response to chloride ($\Delta E \approx 40$ mV), even in the presence of a 100-fold excess of competing anion such as dihydrogenphosphate. This contrasts sharply with the solution responses of the free thread **34**$^+PF_6^-$ and macrocycle **33**, which demonstrate small cathodic shifts in the presence of halides and basic oxyanions, except for **33** with

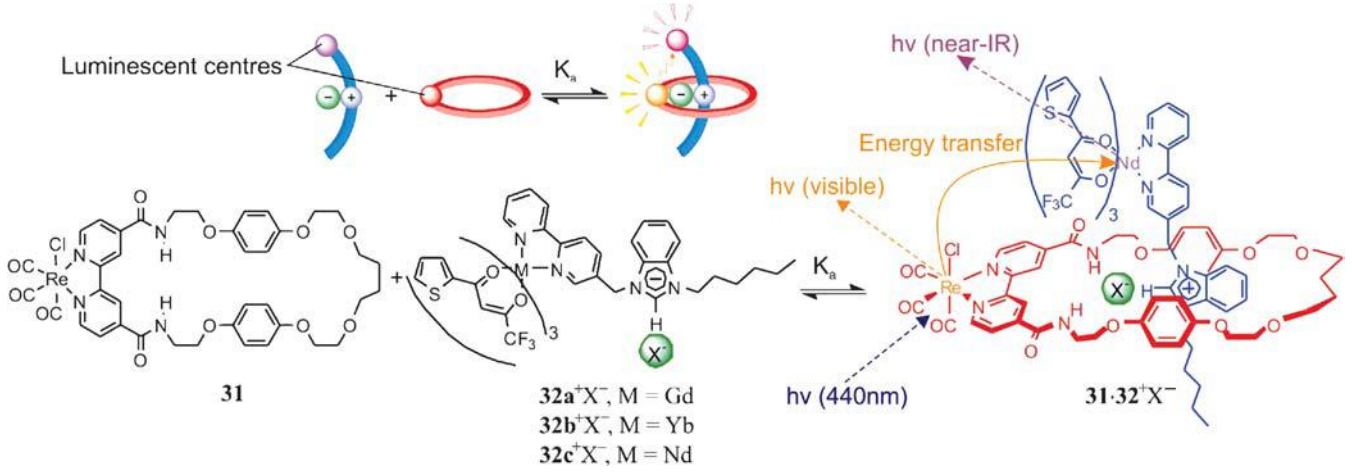

Figure 3.21 Sensing of [2]pseudorotaxane formation through Förster energy transfer. General schematic (top), luminescent macrocycle and thread components (bottom) and pseudorotaxane **31**·**32**$^{+}$X^{-} (right).

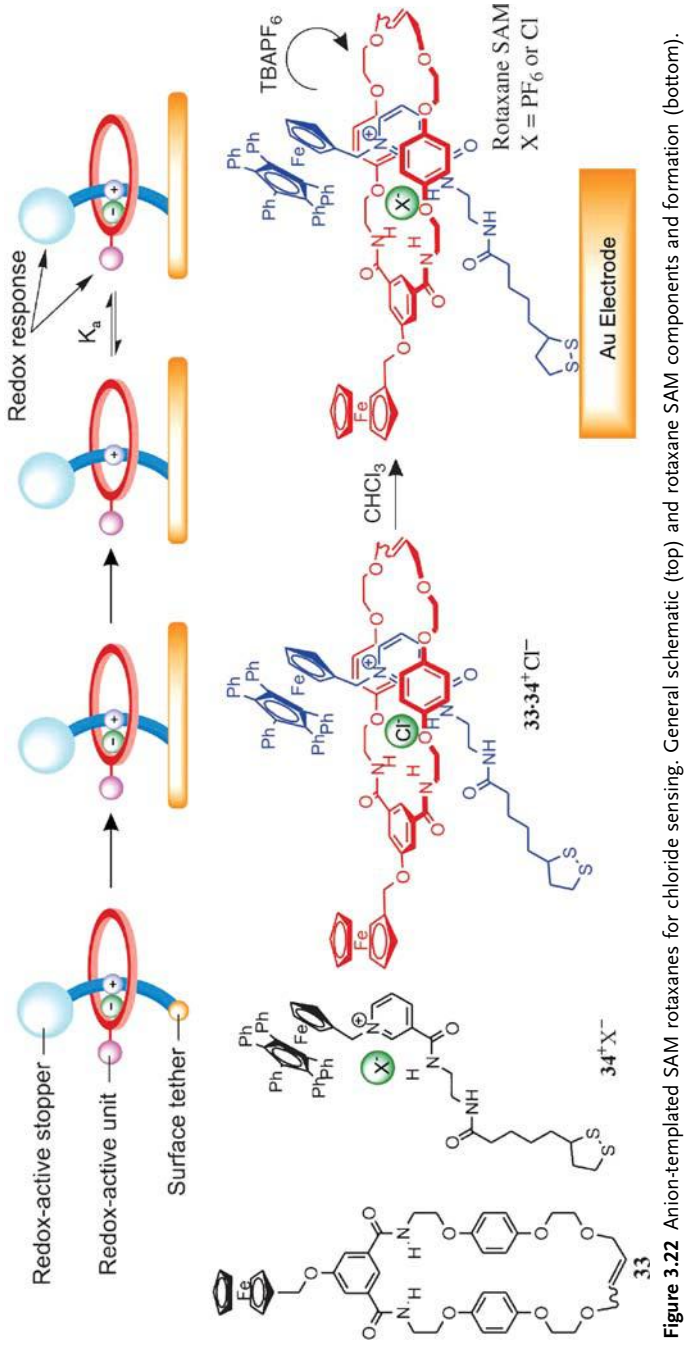

Figure 3.22 Anion-templated SAM rotaxanes for chloride sensing. General schematic (top) and rotaxane SAM components and formation (bottom).

dihydrogenphosphate ($\Delta E \approx 45$ mV) and hydrogensulfate ($\Delta E \approx 15$ mV). This therefore provides another example of the change in selectivity induced by the mutual interpenetration of two components and further demonstrates the ability of this templation methodology to give sophisticated surface-confined species with promising selective electrochemical recognition properties.

To date, the general anion templation synthetic strategy described in this chapter has been exploited in two main areas. The first concerns the removal of the anion template from permanently interlocked molecules, which gives anion receptors demonstrating binding properties dependent upon the presence of a unique three-dimensional hydrogen bond-donating pocket. By including optical and electrochemical readout functionalities and by attaching these derivatives to surfaces, such anion-templated structures have begun to be used for sensory purposes. Second, anion-templated molecular motion in the form of threading has been signaled by luminescence spectroscopic means. This opens the door for molecular machine like devices based on anion recognition processes.

3.9 Summary and Outlook

A comprehensive anionic alternative to existing cation interweaving templation approaches has been developed and exploited in the synthesis of numerous interpenetrated systems. These range from reversible assemblies such as orthogonal complexes and pseudorotaxanes to permanently interlocked compounds such as rotaxanes and catenanes. Removal of the anion template from these permanently interlocked systems leads to novel receptor and sensory behaviors defined by the mutual interpenetration of the two components. These observations underline the general applicability and scope of this novel templation strategy.

This anion templation methodology is, however, currently very much in its infancy; still only a handful of interlocked structures have been obtained and even some threads that have been shown to form pseudorotaxanes are awaiting to be exploited in the construction of permanently interlocked systems. The spectacular progress described in this chapter has been made possible with the exclusive use of halide anions as templates, therefore the application of the whole spectrum of other, more strongly coordinating and structurally complex anions may be expected to open up even more exciting avenues in the field and address current limitations of the methodology. For example, the extension of the currently available threading motifs to uncharged systems would significantly increase its scope.

As shown recently, the application of reversible palladium ligation as the ring-closing reaction in Sauvage's copper-templated catenane synthesis increased the yield from below 30% to quantitative [36]. Certainly, anion-templated synthesis would also benefit from such thermodynamic control. The introduction of reversible reactions compatible with anion supramolecular chemistry may bring a step change in the field.

Further progress in anion-templated rotaxane synthesis is expected with the development of stoppering methods compatible with anion recognition and with broadening of the selection of readily available stoppers of sufficiently large size and various functional groups. Most desirable in this context are functional stoppers such as the electroactive pentaphenylferrocene group from **34**, or photoactive lanthanide complexes from **32**, granting additional degrees of functionality to the resulting rotaxane.

The goal is ultimately to create increasingly sophisticated device-like structures to complement the impressive array of molecular machines already furnished [37] through other templation and self-assembly strategies. We also continue to be fascinated by the potential for these anion-templated architectures to be used for highly selective sensory devices for ionic substrates and we aim to continue the development of such systems. As with the emergence of cationic interweaving templation over two decades ago, however, a huge catalogue of anion-templated structures has yet to be exploited.

References

1 (a) Atwood, J.L., Holman, K.T. and Steed, J.W. (1996) Laying traps for elusive prey: recent advances in the non-covalent binding of anions. *Chem. Commun.*, 1401–1407. (b) for a general introduction, see Sessler, J.L., Gale, P.A. and Cho, W.-S. (2006) *Anion Receptor Chemistry* Royal Society of Chemistry (c) Bianchi, A., Bowman-James, K. and García-España, E. (eds) (1997) *Supramolecular Chemistry of Anions*, Wiley-VCH, New York.

2 Vilar, R. (2003) Anion-templated synthesis. *Angew. Chem. Int. Ed.*, **42**, 1460–1477.

3 Previous accounts: (a) Vickers, M.S. and Beer, P.D. (2007) Anion templated assembly of mechanically interlocked structures. *Chem. Soc. Rev.*, **36**, 211–225. (b) Beer, P.D., Sambrook, M.R. and Curiel, D. (2006) Anion templated assembly of interpenetrated and interlocked structures. *Chem. Commun.*, 2105–2117. (c) Lankshear, M.D. and Beer, P.D. (2006) Strategic anion templation. *Coord Chem. Rev.*, **250**, 3142–3160.

4 Andrievsky, A., Ahuis, F., Sessler, J.L., Vögtle, F., Gudat, D. and Moini, M. (1998) Bipyrrole-based[2]catenane: a new type of anion receptor. *J. Am. Chem. Soc.*, **120**, 9712–9713.

5 For example, Chmielewski, M.J. and Jurczak, J. (2005) Anion recognition by neutral macrocyclic amides *Chem. Eur. J.*, **11**, 6080–6094.

6 (a) Kang, S.O., Llinares, J.M., Powell, D., VanderVelde, D. and Bowman-James, K. (2003) New polyamide cryptand for anion binding. *J. Am. Chem. Soc.*, **125**, 10152–10153. (b) Bisson, A.P., Lynch, V.M., Monahan, M.C. and Anslyn, E.V. (1997) Recognition of anions through NH-π hydrogen bonds in a bicyclic cyclophane – selectivity for nitrate. *Angew. Chem. Int. Ed. Engl.*, **36**, 2340–2342. (c) Schmidtchen, F.P. (1977) Einschluss von Anionen in makrotricyclische quartare Ammoniumsalze. *Angew. Chem.*, **89**, 751–752. (d) Graf, E. and Lehn, J.M. (1976) Anion cryptates: highly stable and selective macrotricyclic anion inclusion complexes. *J. Am. Chem. Soc.*, **98**, 6403–6405. (e) Park, C.H. and Simmons, H.E. (1968) *J. Am. Chem. Soc.*, **90**, 2431–2432.

7 Sasaki, S., Mizuno, M., Naemura, K. and Tobe, Y. (2000) Synthesis and anion-selective complexation of cyclophane-based cyclic thioureas. *J. Org. Chem.*, **65**, 275–283.

8 Anderson, S., Anderson, H.L. and Sanders, J.K.M. (1993) Expanding roles for templates in synthesis. *Acc. Chem. Res.*, **26**, 469–475.

9 Sauvage, J.-P. (1990) Interlacing molecular threads on transition metals: catenands, catenates and knots. *Acc. Chem. Res.*, **23**, 319–327.

10 Kohnke, F.H., Mathias, J.P. and Stoddart, J. (1989) Structure-directed synthesis of new organic materials. *Angew Chem. Int. Ed. Engl. Adv. Mater.*, **28**, 1103–1110.

11 Ashton, P.R., Goodnow, T.T., Kaifer, A.E., Reddington, M.V., Slawin, A.M.Z., Spencer, N., Stoddart, J.F., Vicent, Ch. and Williams, D.J. (1989) A [2]catenane made to order. *Angew. Chem. Int. Ed.*, **28**, 1396–1399.

12 Hübner, G.M., Gläser, J., Seel, Ch. and Vögtle, F. (1999) High-yielding rotaxane synthesis with an anion template. *Angew. Chem. Int. Ed.*, **38**, 383–386.

13 Seel, Ch. and Vögtle, F. (2000) Templates, "wheeled reagents" and a new route to rotaxanes by anion complexation: the trapping method. *Chem. Eur. J.*, **6**, 21–24.

14 Shukla, R., Deetz, M.J. and Smith, B.D. (2000) [2]Rotaxane with a cation binding wheel. *Chem. Commun.*, 2397–2398.

15 Mahoney, J.M., Shukla, R., Marshall, R.A., Beatty, A.M., Zaijcek, J. and Smith, B. (2002) Template conversion of a crown ether-containing macrobicycle into [2] rotaxanes. *J. Org. Chem.*, **67**, 1436–1440.

16 Deetz, M.J., Shukla, R. and Smith, B.D. (2002) Recognition-directed assembly of salt-binding [2]rotaxanes, *Tetrahedron*, **58**, 799–805.

17 Schalley, Ch.A., Silva, G., Nising, C.F. and Linnartz, P. (2002) Analysis and improvement of an anion-templated rotaxane synthesis. *Helv. Chim. Acta*, **85**, 1578–1596.

18 Ghosh, P., Mermagen, O. and Schalley, Ch.A. (2002) Novel template effect for the preparation of [2]rotaxanes with functionalised centre pieces. *Chem. Commun.*, 2628–2629.

19 Arunkumar, E., Forbes, Ch.C., Noll, B.C. and Smith, B.D. (2005) Squaraine-derived rotaxanes: sterically protected fluorescent near-IR dyes. *J. Am. Chem. Soc.*, **127**, 3288–3289.

20 Mohr, B., Weck, M., Sauvage, J.-P. and Grubbs, R.H. (1997) High-yield synthesis of [2]catenanes by intramolecular ring-closing metathesis. *Angew. Chem. Int. Ed.*, **36**, 1308–1310.

21 Kavallieratos, K., Bertao, C.M. and Crabtree, R.H. (1999) Hydrogen bonding in anion recognition: a family of versatile, nonpreorganized neutral and acyclic receptors. *J. Org. Chem.*, **64**, 1675–1683.

22 Wisner, J.A., Beer, P.D. and Drew, M.G.B. (2001) A demonstration of anion templation and selectivity in pseudorotaxane formation. *Angew. Chem. Int. Ed.*, **40**, 3606–3609.

23 Wisner, J.A., Beer, P.D., Drew, M.G.B. and Sambrook, M.R. (2002) Anion-templated rotaxane formation. *J. Am. Chem. Soc.*, **124**, 12469–12476.

24 Sambrook, M.R., Beer, P.D., Wisner, J.A., Paul, R.L., Cowley, A.R., Szemes, F. and Drew, M.G.B. (2005) Anion-templated assembly of pseudorotaxanes: importance of anion template, strength of ion-pair thread association and macrocycle ring size. *J. Am. Chem. Soc.*, **127**, 2292–2302.

25 Wisner, J.A., Beer, P.D., Berry, N.G. and Tomapatanaget, B. (2002) Anion recognition as a method for templating pseudorotaxane formation. *Proc. Natl. Acad. Sci. USA*, **99**, 4983–4986.

26 Lankshear, M.D., Evans, N.H., Bayly, S.R. and Beer, P.D. (2007) Anion-templated calix[4]arene-based pseudorotaxanes and catenanes. *Chem. Eur. J.*, **13**, 3861–3870.

27 Curiel, D., Beer, P.D., Paul, R.L., Cowley, A.R., Sambrook, M.R. and Szemes, F. (2004) Halide anion directed assembly of luminescent pseudorotaxanes. *Chem. Commun.*, 1162–1163.

28 Beer, P.D., Timoshenko, V., Maestri, M., Passaniti, P. and Balzani, V. (1999) Anion recognition and luminescent sensing by new ruthenium(II) and rhenium(I) bipyridyl calyx[4]diquinone receptors. *Chem. Commun.*, 1755–1756.

29 Grubbs, R.H., Miller, S.J. and Fu, G.C. (1995) Ring-closing metathesis and related processes in organic synthesis. *Acc. Chem. Res.*, **28**, 446–452.

30 Sambrook, M.R., Beer, P.D., Lankshear, M.D., Ludlow, R.F. and Wisner, J.A. (2006) Anion-templated assembly of [2] rotaxanes. *Org. Biol. Chem.*, **4**, 1529–1538.

31 Sambrook, M.R., Beer, P.D., Wisner, J.A., Paul, R.L. and Cowley, A.R. (2004) Anion-templated assembly of a [2]catenane. *J. Am. Chem. Soc.*, **126**, 15364–15365.

32 Ng, K.-Y., Cowley, A.R. and Beer, P.D. (2006) Anion templated double cyclization assembly of a chloride selective [2]catenane. *Chem. Commun.*, 3676–3678.

33 Curiel, D. and Beer, P.D. (2005) Anion directed synthesis of a hydrogensulfate selective luminescent rotaxane. *Chem. Commun.*, 1909–1911.

34 Sambrook, M.R., Curiel, D., Hayes, E.J., Beer, P.D., Pope, S.J. and Faulkner, S. (2006) Sensitized near infrared emission from lanthanides via anion-templated assembly of d-f heteronuclear [2] pseudorotaxanes. *New J. Chem.*, **30**, 1133–1136.

35 Bayly, S.R., Gray, T.M., Chmielewski, M.J., Davis, J.J. and Beer, P.D. (2007) Anion templated surface assembly of a redox-active sensory rotaxane. *Chem. Commun.*, **2234–2236.**

36 Dietrich-Buchecker, Ch., Colasson, B., Fujita, M., Hori, A., Geum, N., Sakamoto, S., Yamaguchi, K. and Sauvage, J.-P. (2003) Quantitative formation of [2]catenanes using copper(I) and palladium(II) as templating and assembling centers: the entwining route and the threading approach. *J. Am. Chem. Soc.*, **125**, 5717–5725.

37 (a) Kay, E.R., Leigh, D.A. and Zerbetto, F. (2007) Synthetic molecular motors and mechanical machines. *Angew. Chem. Int. Ed.*, **46**, 72–191. (b) Sauvage, J.-P. and Dietrich-Buchecker, C. (eds) (1999) *Molecular Catenanes, Rotaxanes and Knots: a Journey Through the World of Molecular Topology*, Wiley-VCH, Weinheim.

4
Synthetic Nanotubes from Calixarenes

Dmitry M. Rudkevich[†] *and Voltaire G. Organo*

4.1
Introduction

Synthetic nanotubes represent a novel type of molecular containers. In supramolecular chemistry, they are still overshadowed by more popular cavitands, carcerands and self-assembling capsules [1,2]. They also have not received much attention compared with the similarly shaped carbon nanotubes [3] and biologically relevant ion channels [4]. At the same time, synthetic nanotubes possess unique dimensions and topology and, as a consequence, different and interesting complexation properties. They also offer a variety of applications in chemistry, nanotechnology and medicine. One important feature of nanotubes is the ability to align multiple guest species in one dimension (1D), which is useful for ion and molecular transport, nanowires and information flow. Other potential applications include using nanotubes as reaction vessels and molecular cylinders for separation and storage.

In recent years, a number of general reviews have appeared describing approaches towards the preparation and characterization of organic nanotubes [5]. This chapter will focus on nanotubes that are based on calixarenes. Calixarenes, cyclic oligomers of phenols and aldehydes, play a special role in molecular recognition [6]. They have yielded a great number of excellent receptors for ions and neutral molecules. In particular, calixarenes appear to be useful in the design of molecular containers [1,2]. We will discuss the synthesis of calixarene-based nanotubes and their emerging host–guest properties, including encapsulation, the guest dynamics and exchange and potential applications.

Research on synthetic nanotubes has been inspired, in many ways, by recent successes with ion channels on the one hand and single-walled carbon nanotubes (SWNTs) on the other. As valuable supplements, organic synthesis offers robust and well-defined tubular structures, with a wide variety of sizes. It also helps to control the nanotube length. Through smart molecular design, it is also possible to prepare stable host–guest complexes. All these features are not easy to achieve for ion channels and SWNTs.

Organic Nanostructures. Edited by Jerry L. Atwood and Jonathan W. Steed
Copyright © 2008 WILEY-VCH Verlag GmbH & Co. KGaA, Weinheim
ISBN: 978-3-527-31836-0

Another issue is characterization. The functions of synthetic ion channels are commonly assessed by electrophysiological planar-bilayer voltage-clamp techniques, fluorimetric assays on liposomes and heteronuclear and solid-state NMR spectroscopy. Transmission electron microscopy is used to study the location of molecules inside SWNTs in the solid state. Solution studies with SWNTs are a great challenge because of their poor solubility. As well-defined organic structures, synthetic nanotubes overcome these difficulties. Their complexes can be prepared and handled by standard organic chemistry protocols and studied by conventional organic spectroscopies.

4.2 Early Calixarene Nanotubes

Early calix[4]arene-based nanotubes were reported by Shinkai and coworkers [7]. Taking advantage of the dynamic behavior of metal cation complexes with *1,3-alternate* calix[4]arenes, they connected several such calixarenes to form nanotubes **1**–**4** (Figure 4.1). Conceptually, nanotubes **1**–**4** would allow small metal cations to tunnel through its π-basic interior.

Complexation experiments with $Ag^+CF_3SO_3^-$ revealed the presence of a 1 : 1 Ag^+ ion complex with calix[4]tube **2**. Analysis of the variable-temperature ^1H NMR spectrum of the complex suggested that the Ag^+ ion is delocalized between two calixarenes.

The authors proposed that the metal cation oscillates between metal-binding sites in calix[4]tubes in two possible modes: intracalixarene metal tunneling and intercalixarene metal hopping (Figure 4.2). This dynamic behavior, however, was not observed in the complexation with calix[4]tube **1**. Instead, a mixture of free tube **1** and the 1 : 2 **1** Ag^+ complex was found in the ^1H NMR spectra. It was suggested that the *para* substituents used to connect the two calixarenes interfered with the cation–π interactions, thus suppressing the metal tunneling. In this case, the Ag^+ ions were said to be localized at the edges of the tube, interacting with the calixarene rings and the propyloxy-oxygen groups through cation–π and electrostatic $O\cdots Ag^+$ interactions, respectively.

Similarly, there was no evidence of metal tunneling in complexation studies with calix[4]tube **3** and no data were reported for longer tube **4**. A 1:1 mixture of **3** and $Ag^+CF_3SO_3^-$ yielded three different species: free **3**, **3** Ag^+ and **3** $(Ag^+)_2$ in a 1:2:1 ratio. This result implies that Ag^+ is bound to **3** according to simple probability. The lack of metal tunneling was suspected to be the result of several structural features of **3**. These include the *para* substitution of phenyl groups in the calixarene units, the increased distance between two calixarene units relative to other structures and the nonionophoric bridges connecting the calixarene units.

While Shinkai's nanotubes were only 2–4 nm long and of molecular weight up to 1500 Da, it should be possible to prepare much longer structures utilizing the same calixarene precursors. These pioneering studies, initiated in the early 1990s, triggered intense research on calixarene-based tubular (nano)structures for metal ion complexation, tunneling and transport [8–12].

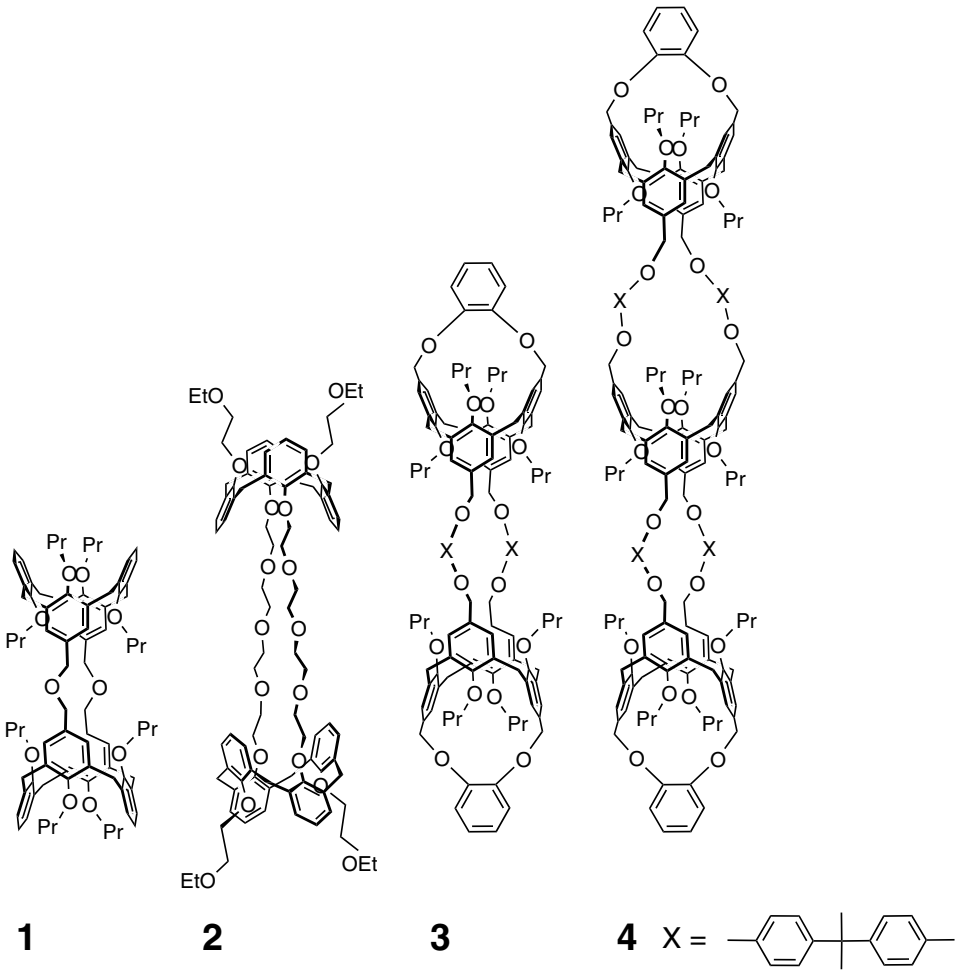

Figure 4.1 Early calix[4]arene nanotubes [7].

4.3
Metal Ion Complexes with Calixarene Nanotubes

Kim and coworkers reported multiply connected *1,3-alternate* calix[4]arene tubes **5** (Figure 4.3), in which the terminal calixarene units were capped with crown ethers [11]. In this design, however, K^+ or Cs^+ cations were bound in tubes **5** ($m = 1, 2$) at the end-calixcrown "stoppers" and metal shuttling was not observed. The X-ray crystal structure of the biscalix[4]crown **5** ($n = 1$, $m = 1$) with K^+ ions revealed that electrostatic interactions between the oxygen donor atoms of the crown ether ring and the metal cation play a major role in entrapping the metal ion whereas the cation–π interaction plays a minor role.

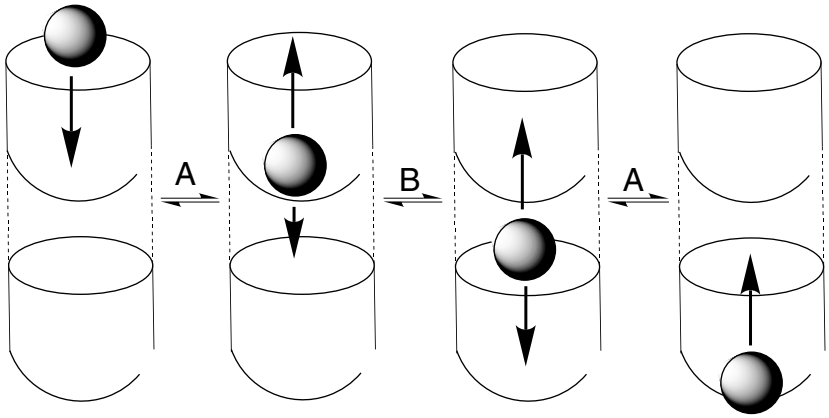

Figure 4.2 Proposed intracalixarene metal tunneling (route A) and intercalixarene metal hopping (route B) [7].

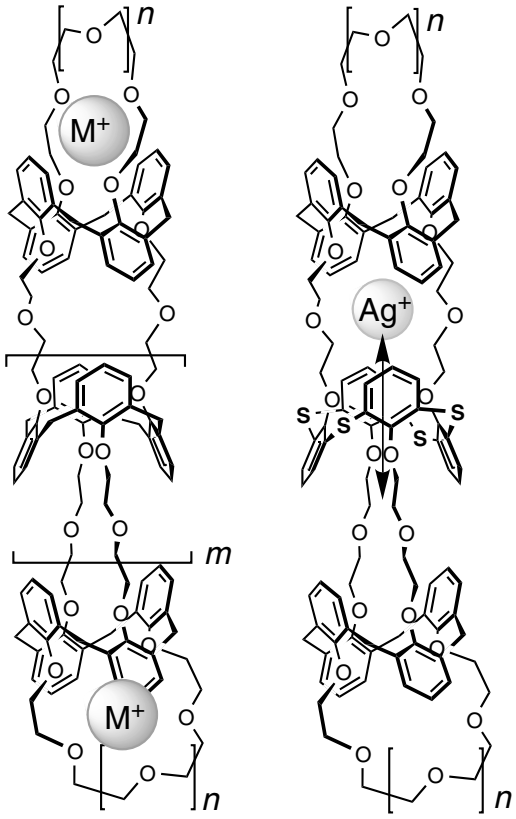

5 **6**

Figure 4.3 Calixcrown nanotubes for metal ions complexation and tunneling [11,12].

The apparent problem with the calixarene nanotubes was the lack of strong cation–π interactions within the interior. Monitoring trapped cationic guests by conventional NMR spectroscopy in these nanotubes was also difficult.

A structural analog of nanotubes **5** was recently prepared which possesses a calixarene unit with higher affinity to metal cations [12]. Nanotubes **6** ($n = 1, 2$) contained thiacalix[4]arene in the middle and the Ag^+ cation was found to be entraped in this central unit in a 1 : 1 fashion (Figure 4.3). In addition to the calixarene aromatic rings, the sulfur atoms provided supplementary coordination sites for transition metal ions. Variable-temperature ^1H NMR spectroscopy revealed that the Ag^+ oscillates through the thiacalixarene and cation–π interactions were important in this case. With some further modifications, it should be possible to synthesize polymeric analogs of tube **6**, inside which Ag^+ ions can freely shuttle [12].

4.4 Nanotubes for NO_x Gases

Synthetic nanotubes have recently been introduced that possess much more pronounced cation–π features. These are based on reversible chemistry between calix[4]arenes and NO_2/N_2O_4 gases [13,14]. NO_2 is paramagnetic and exists in equilibrium with its dimer N_2O_4. N_2O_4 disproportionates to ionic $NO^+NO_3^-$ while interacting with aromatic compounds. It was found that tetrakis-*O*-alkylated calix[4]arenes, e.g. **7**, react with NO_2/N_2O_4 to form very stable ($K_{assoc} \gg 10^6\ M^{-1}$), charge-transfer calix-nitrosonium (NO^+) complexes **8**. In these, NO^+ cations are strongly encapsulated within the π-electron-rich calix[4]arene tunnel (Figure 4.4). This phenomenon was used in the design of calixarene nanotubes.

In nanotubes **9**–**12**, *1,3-alternate* calix[4]arenes were rigidly connected from both sides of their rims with pairs of diethylene glycol linkers (Figures 4.5 and 4.6) [15–17]. In this conformation, two pairs of phenolic oxygens are oriented in opposite directions, providing diverse means to enhance modularly the tube length. The nanotubes possess defined inner tunnels 6 Å in diameter and approximately 15, 25, 35 and 45 Å in length for **9**, **10**, **11** and **12**, respectively. Tubes **11** and **12** have molecular

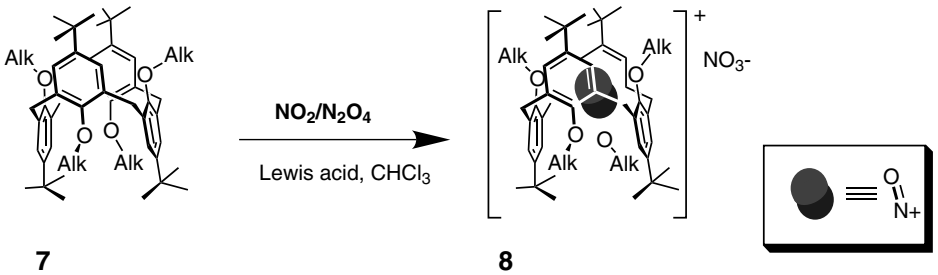

7 **8**

Figure 4.4 Simple calix[4]arenes and their supramolecular interactions with NO_2/N_2O_4 gases; generation of nitrosonium complexes [13].

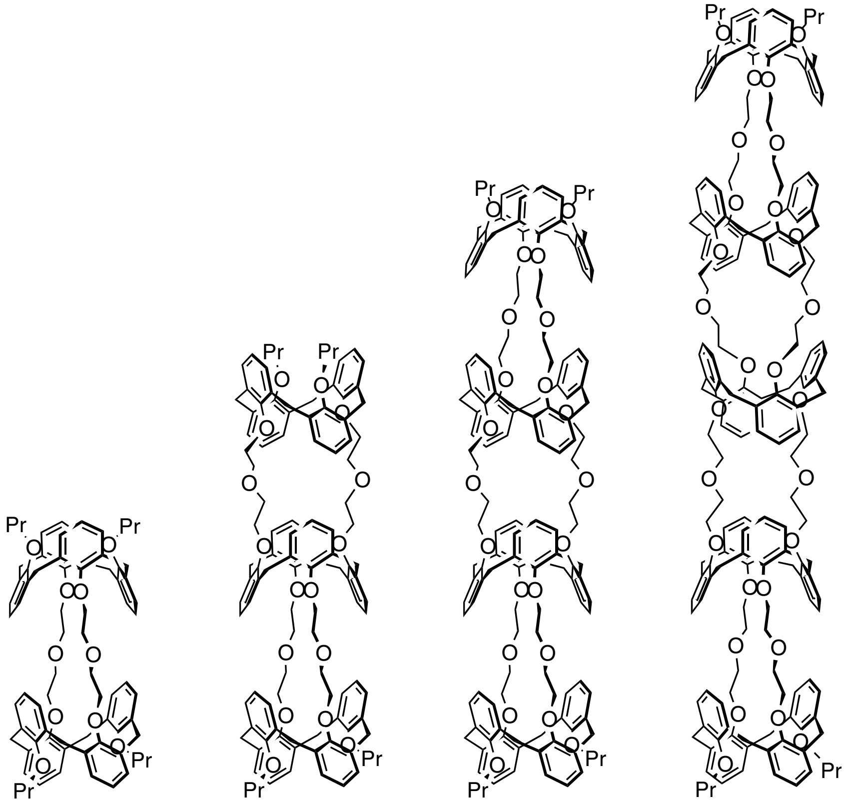

9 **10** **11** **12**

Figure 4.5 Synthetic nanotubes for entrapment of NO_x gases [15–17].

weights of ∼2.3 and 2.8 kDa, respectively. These features place them among the largest nonpolymeric, synthetic molecular containers known to date [1].

The synthesis was based on a straightforward strategy, which incorporated reliable Williamson-type alkylations and provided yields as high as 70–80% (Scheme 4.1). For example, the synthesis of trimeric tube **10** was accomplished in 70% yield by the coupling of tetratosylate **13** with two equivalents of diol **14** in boiling THF with NaH as a base. Tube **11**, which contains four linked calixarenes, was prepared by reaction of biscalixarene diol **15** with ditosylate **16** in 64% yield using NaH and K_2CO_3 in THF. Finally, reaction of two equivalents of diol **16** with tetratosyate **13** under the same conditions afforded pentameric nanotube **12** in a remarkable 82% yield [17].

Addition of excess NO_2/N_2O_4 to nanotubes **9**–**12** in $(CHCl_2)_2$ in the presence of stabilizing Lewis acids ($SnCl_4$ or $BF_3{\cdot}Et_2O$) resulted in quantitative formation of nitrosonium complexes **9**$\cdot(NO^+)_2$–**12**$\cdot(NO^+)_5$ (Figure 4.7). Similar complexes formed when nanotubes **9**–**12** were mixed with a commercially available nitrosonium salt,

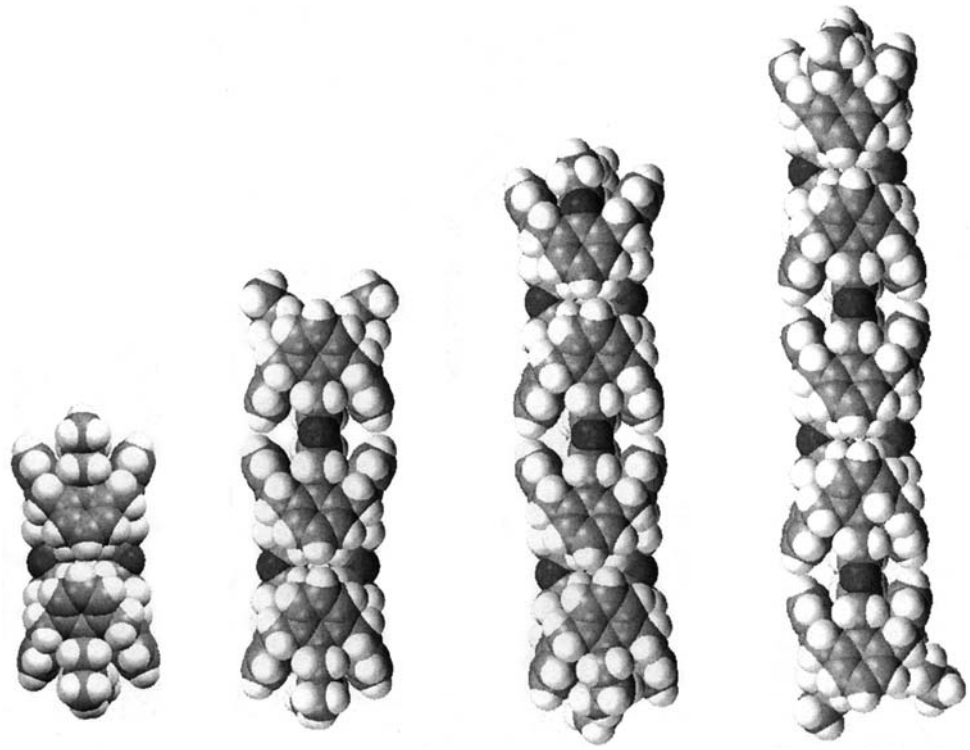

Figure 4.6 Molecular models of nanotubes **9**–**12**.

$NO^+SbF_6^-$, in $(CHCl_2)_2$. Complexes **9**·$(NO^+)_2$–**12**·$(NO^+)_5$ were identified by absorption, IR and ^1H NMR spectroscopy. Of particular importance is the characteristic deep purple color. The broad charge-transfer bands responsible for this were observed at $\lambda_{max} \approx 550$ nm in the absorption spectra of all these nanotubes. The charge transfer occurs only when NO^+ guests are tightly entrapped inside the calixarene cavities. Accordingly, the filling process can be monitored visually.

Upon stepwise addition of NO_2/N_2O_4 or $NO^+SbF_6^-$ in $(CDCl_2)_2$, the ^1H NMR signals of empty tubes **9**–**12** and complexes **9**·$(NO^+)_2$–**12**·$(NO^+)_5$ can be seen separately and in slow exchange. The guests presence and location inside nanotubes **9**·$(NO^+)_2$–**12**·$(NO^+)_5$ was deduced from conventional ^1H NMR, COSY and NOESY experiments. Chemical shifts of the Ar−O−CH_2 and CH_2−O−CH_2 protons and, to lesser extent, the aromatic protons are very sensitive to the encapsulation. In addition to the charge transfer, strong cation–dipole interactions between the calixarene oxygen atoms and the entrapped NO^+ take place. Through ^1H NMR titration experiments and molecular modeling, the stoichiometry of the nanotube complexes was unumbigously established: they possess one NO^+ guest per calixarene unit.

FTIR spectra allowed unique information to be obtained on the bonding of multiple NO^+ species inside tubes **9**·$(NO^+)_2$–**12**·$(NO^+)_5$ in solution [17]. From the literature, nitrosonium salts NO^+Y^- ($Y^- = BF_4^-$, PF_6^-, AsF_6^-) showed a single

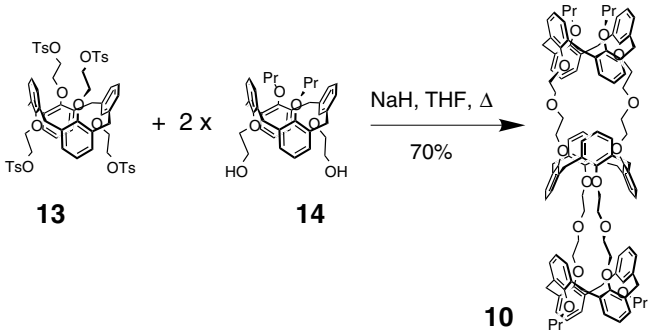

13 **14** **10**

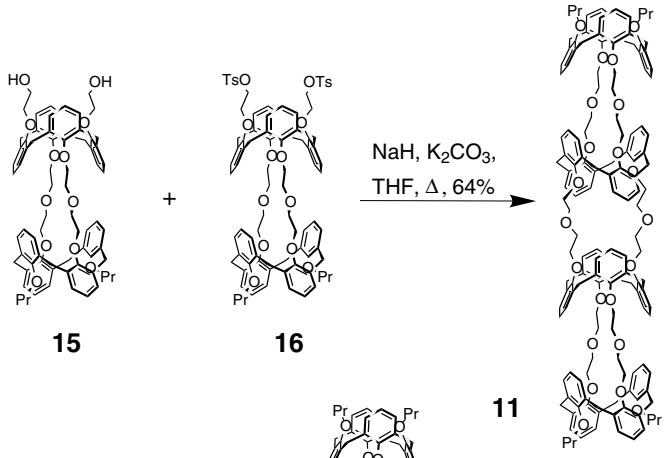

15 **16** **11**

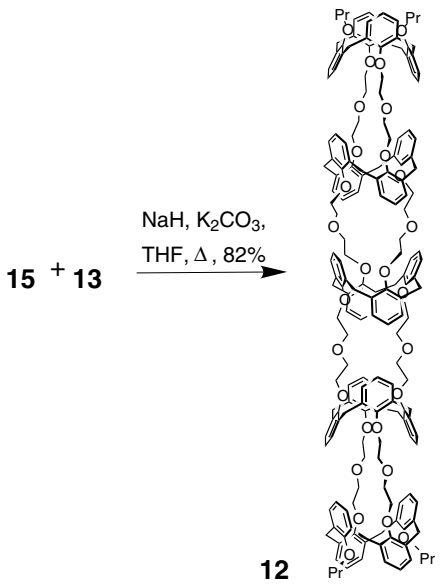

12

Scheme 4.1 Preparation of calix[4]arene-based nanotubes [17].

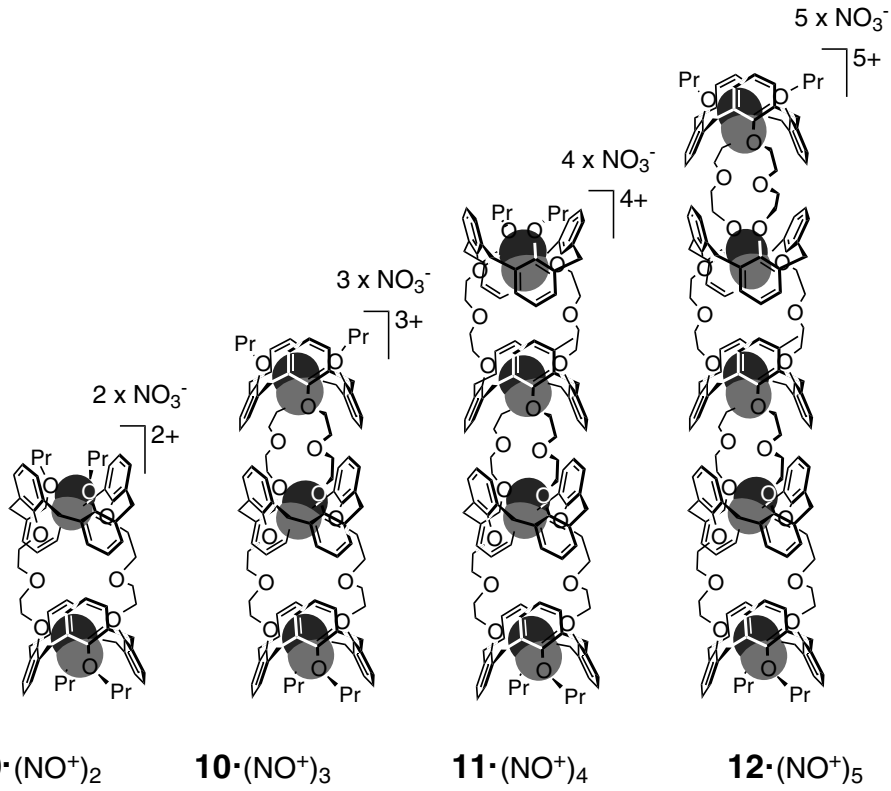

Figure 4.7 Nanotubes **9**–**12** disproportionate NO_2/N_2O_4 gases and entrap multiple NO^+ cations.

stretching band at $\nu(NO^+) = 2270\,cm^{-1}$ in CH_3NO_2 solutions and the stretching frequency of the neutral diatomic NO gas was $\nu(NO) = 1876\,cm^{-1}$. In calixarene–NO^+ complexes **8**, the NO^+ band significantly shifted ($\Delta\nu = 312\,cm^{-1}$) to the lower energies, compared to free NO^+ cation and appeared at $\nu(NO^+) = 1958\ cm^{-1}$ in $(CHCl_2)_2$. This is due to strong electron donor–acceptor interactions between the encapsulated NO^+ and π-electron-rich aromatic walls of the calixarene. Dimeric complex **9** $(NO^+)_2$ also exhibited similar shifts for the NO^+ guests at $\nu(NO^+) = 1958\,cm^{-1}$. At the same time, longer tubes **10**·$(NO^+)_3$–**12**·$(NO^+)_5$ clearly showed two absorption bands at $\nu(NO^+) = 1958$ and $1940\,cm^{-1}$ in $(CHCl_2)_2$. For trimeric tube **10**·$(NO^+)_3$, these two bands have a comparable intensity, whereas in longer tubes **11**·$(NO^+)_4$ and **12**·$(NO^+)_5$ the band at $\nu(NO^+) = 1940\,cm^{-1}$ dominates. This band was assigned to the NO^+ guest(s), which are situated in the middle of the tubes. Apparently, they are somewhat more strongly bound to the nanotubes walls.

One possible explanation may be a participation of the glycol CH_2OCH_2 oxygens in the complexation process. The FTIR data strongly suggest the *anti-gauche* conformational transition of these CH_2OCH_2 chains upon complexation, so their oxygens

appear in close proximity to the complexed NO^+ and thus contribute to dipole–cation interactions [17]. Cooperativity through allosteric effects is also possible. It may be the result of multiple guests aligning in one dimension, which brings an order that cannot be achieved for shorter complexes.

Filled nanotubes **9**·$(NO^+)_2$–**12**·$(NO^+)_5$ were stable in dry solution at room temperature for hours, but could readily dissociate upon addition of H_2O or alcohol, quantitatively reproducing free **9–12**. The process, however, is not reversible: the released NO^+ species are now converted to nitrous acid and complexes **9**·$(NO^+)_2$–**12**·$(NO^+)_5$ cannot be regenerated.

However, it was further found that 18-crown-6 could reversibly remove the encapsulated NO^+ species. It is known that crown ethers form stable complexes with NO^+. When ~4 equiv. of 18-crown-6 were added to $(CDCl_2)_2$ solutions of **9**·$(NO^+)_2$ and **10**·$(NO^+)_3$, empty nanotubes **9**·and **10**, respectively, regenerated within minutes and the deep-purple color disappeared. Interestingly, further addition of $SnCl_4$ to the same solutions fully restores complexes **9**·$(NO^+)_2$ and **10**·$(NO^+)_3$. Apparently, an excess $SnCl_4$ replaces NO^+ from the crown ether moiety and the latter goes back to the calixarene units of the nanotubes. This observation is important, since in this case foreign species can be replaced and returned back without decomposition or changing the solution polarity.

Modeling suggests that NO^+ can enter and leave the nanotube either through its ends or the middle gates between the calixarene modules. The approach and exit through the ends appears to be less hindered. The middle gates between the calixarene units become narrower due to the glycol conformational changes from *anti* to *gauche* upon complexation. The encapsulated NO^+ species should also avoid electrostatic repulsions with each other. Most probably, the tube filling and release occurs through the guest tunneling along the interior.

In the solid state, longer nanotubes **10** (but not tubes **9**) pack head-to-tail, in straight rows, resulting in infinitely long cylinders (Figure 4.8) [16]. The neighboring nanocylinders are aligned parallel to each other. In each nanocylinder, molecules **10** are twisted by 90° relative to each other and the Ar—O—Pr propyl groups effectively occupy the voids between the adjacent molecules. In such an arrangement, the intermolecular distance between two neighboring tubes in the nanocylinder is ~6 Å. The nanocylinders are separated from each other by ~9 Å. This supramolecular order comes with the tube length and is without precedent for conventional, shorter calixarenes. The unique linear nanostructures maximize their intermolecular van der Waals interactions in the crystal through the overall shape simplification. Such a unique arrangement resembles that of SWNT bundling.

Among possible applications of nanotubes **9–12** are nanowires and also optical sensors for NO_x. Chemical fixation of NO_x is also of great interest. Indeed, the tubes can be used for molecular storage of active nitrosonium and act as size–shape-selective nitrosating reagents [14,15]. In addition, they can be used for generating NO gas.

In a one-electron reduction scheme involving the calixarene-NO^+ complexes **8**, **9**·$(NO^+)_2$ and **10**·$(NO^+)_3$ and simple hydroquinone, NO was smoothly released and free calixarenes **7**, **9** and **10** were quantitatively regenerated (see, for example,

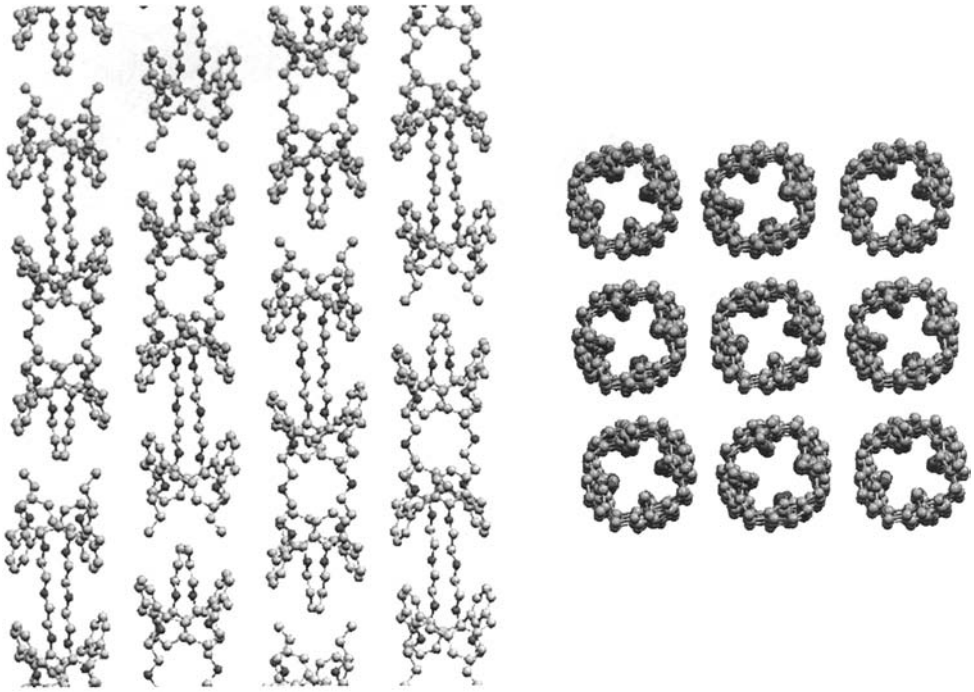

Figure 4.8 Solid-state packing of nanotube **10**, side and top views (from the X-ray structure) [16].

Figure 4.9) [18]. In detail, when a ~20-fold excess of hydroquinone was added to the $(CDCl_2)_2$ solutions of nitrosonium filled nanotubes **9**·$(NO^+)_2$ and **10**·$(NO^+)_3$, the color changed from deep purple to yellow. The ^1H NMR spectrum clearly showed the quantitative regeneration of the empty nanotubes **9** and **10**. The NO release could be visually detected and identified by UV spectrophotometry. The use of calixarene nanotubes, capable of storing *multiple* NO^+ species, could potentially lead to interesting NO-releasing materials with a high gas capacity.

4.5
Self-assembling Structures

Solid-state self-assembling nanotubes were recently published that are based on calixarenes [19–21]. Although their stability and host–guest behavior in solution still remain to be investigated, it should be possible to use preorganized calixarene cavities for molecular encapsulation, separation and storage. It must be remembered, however, that self-assembling nanotubes are stable only under specific, rather mild conditions, which may not be suitable for some applications. Another important but still unresolved issue is control over their length.

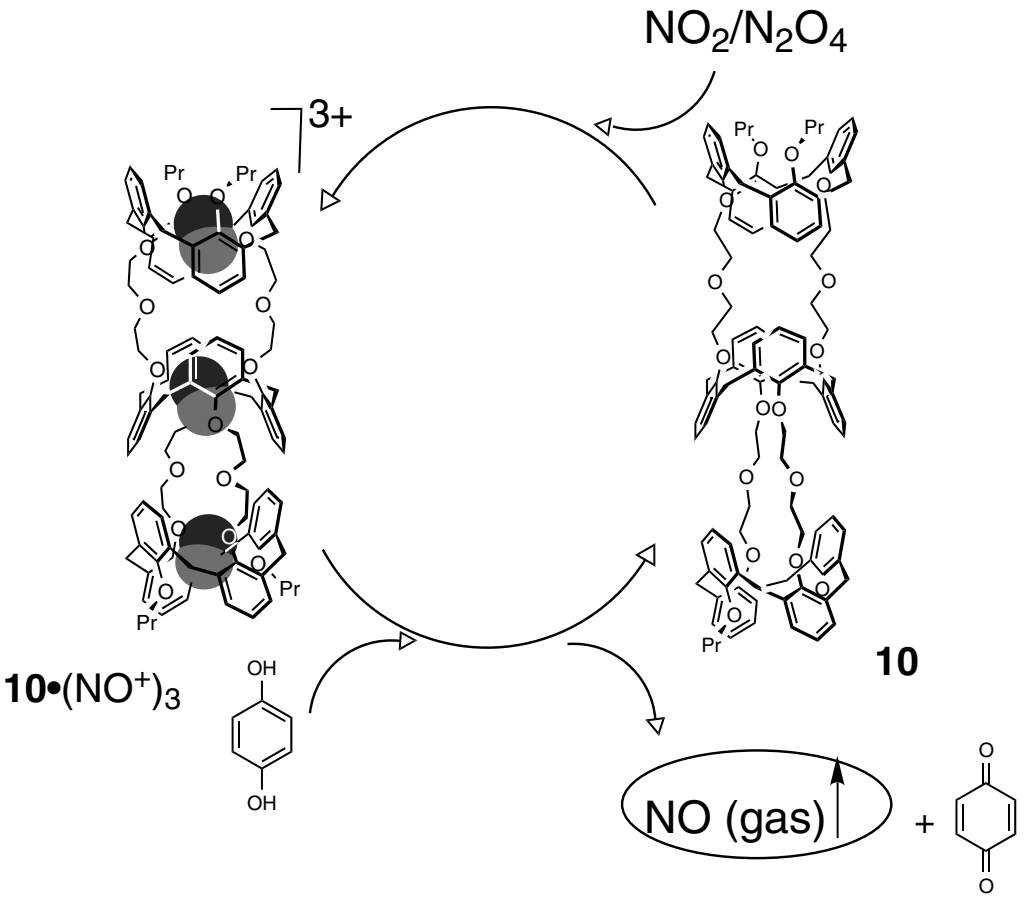

Figure 4.9 Calixarene nanotubes can be used for generation of NO gas [18].

4.6 Conclusions and Outlook

Synthetic nanotubes are promising molecular containers. Their geometric features and actual nanodimensions clearly place them in a unique position compared with conventional molecular containers. Described here, calixarene-based nanotubes simultaneously entrap multiple guests in a 1D fashion. The guest exchange mechanism is also different, since nanotubes are open from both ends and do not require dissociation [22]. This leads to interesting host–guest dynamics and opens the door to such applications as 1D ion mobility for transport and nanowires, inner-space reactions with subsequent product release and also high-capacity porous materials for molecular separation and storage. This also establishes an internal order that

cannot be achieved for conventional encapsulation complexes and even may influence the binding strength.

In contrast to SWNTs and ion channels, conventional organic spectroscopy can be used to study the complexation processes and monitor guest behavior within the interior.

Among the future goals will be the synthesis of even more sophisticated nanotubes. There is a need to achieve higher kinetic and thermodynamic stabilities of the encapsulation complexes. It also remains to be seen how the encapsulated guests interact or even react with each other and the nanotube walls and whether their properties in a confined environment are different from those in bulk.

Acknowledgment

The National Science Foundation is acknowledged for financial support.

References

1 (a) Cram, D.J. and Cram, J.M. (1994) *Container Molecules and their Guests*, Royal Society of Chemistry. (b) Rudkevich, D.M. (2002) *Bull. Chem. Soc. Jpn.*, **75**, 393–413. (c) Rudkevich, D.M. (2005) *Functional Artificial Receptors* (eds T. Shrader and A.D. Hamilton), Wiley-VCH, Weinheim, 257–298.

2 (a) Purse, B.W. and Rebek, J. Jr. (2005) *Proc. Natl. Acad. Sci. USA*, **102**, 10777–10782. (b) Jasat, A. and Sherman, J.C. (1999) *Chem. Rev.*, **99**, 931–967. (c) Warmuth, R. and Yoon, J. (2001) *Acc. Chem. Res.*, **34**, 95–105. (d) Collet, A., Dutasta, J.-P., Lozach, B. and Canceill, J. (1993) *Top. Curr. Chem.*, **165**, 103–129. (e) Rebek, J. Jr. (2005) *Angew. Chem. Int. Ed.*, **44**, 2068–2078. (f) Hof, F., Craig, S.L., Nuckolls, C. and Rebek, J. Jr. (2002) *Angew. Chem. Int. Ed.*, **41**, 1488–1508

3 Britz, D.A. and Khlobystov, A.N. (2006) *Chem. Soc. Rev.*, **35**, 637–659.

4 (a) Sisson, A.L., Shah, M.R., Bhosale, S. and Matile, S. (2006) *Chem. Soc. Rev.*, **35**, 1269–1286. (b) Sakai, N., Mareda, J. and Matile, S. (2005) *Acc. Chem. Res.*, **38**, 79–87. (c) Matile, S., Som, A. and Sorde, N. (2004) *Tetrahedron*, **60**, 6405–6435.

5 (a) Bong, D.T., Clark, T.D., Granja, J.R. and Ghadiri, M.R. (2001) *Angew. Chem. Int. Ed.*, **40**, 988–1011. (b) Pasini, D. and Ricci, M. (2007) *Curr. Org. Synth.*, **4**, 59–80. (c) Baklouti, L., Harrowfield, J., Pulpoka, B. and Vicens, J. (2006) *Mini-Rev. Org. Chem.*, **3**, 356–386.

6 (a) Asfari, Z., Böhmer, V., Harrowfield, J. and Vicens, J. (eds) (2001) *Calixarene 2001*, Kluwer. Dordrecht (b) Gutsche, C.D. (1998) *Calixarenes Revisited*, Royal Society of Chemistry, Cambridge.

7 (a) Ikeda, A. and Shinkai, S. (1994) *J. Chem. Soc., Chem. Commun.*, 2375–2376. (b) Ikeda, A., Kawaguchi, M. and Shinkai, S. (1997) *Anal. Quim. Int. Ed.*, **93**, 408–414.

8 (a) Khomich, E., Kasparov, M., Vatsouro, I., Shokova, E. and Kovalev, V. (2006) *Org. Biomol. Chem.*, **4**, 1555–1560. (b) Gac, S.L., Zeng, X., Reinaud, O. and Jabin, I. (2005) *J. Org. Chem.*, **70**, 1204–1210.

9 (a) Matthews, S.E., Schmitt, P., Felix, V., Drew, M.G.B. and Beer, P.D. (2002) *J. Am. Chem. Soc.*, **124**, 1341–1353. (b)

Matthews, S.E., Felix, V., Drew, M.G.B. and Beer, P.D. (2003) *Org. Biomol. Chem.*, **1**, 1232–1239. (c) Webber, P.R.A., Cowley, A., Drew, M.G.B. and Beer, P.D. (2003) *Chem. Eur. J.*, **9**, 2439–2446 (d) Matthews, S.E., Felix, V., Drew, M.G.B. and Beer, P.D. (2001) *New J. Chem.*, **25**, 13551358.

10 Perez-Adelmar, J.-A., Abraham, H., Sanchez, C., Rissanen, K., Prados, P. and de Mendoza, J. (1996) *Angew. Chem. Int. Ed.*, **35**, 1009–1011.

11 (a) Kim, S.K., Sim, W., Vicens, J. and Kim, J.S. (2003) *Tetrahedron Lett.*, **44**, 805–809. (b) Kim, S.K., Vicens, J., Park, K.-M., Lee, S.S. and Kim, J.S. (2003) *Tetrahedron Lett.*, **44**, 993–997.

12 Kim, S.K., Lee, J.K., Lee, S.H., Lim, M.S., Lee, S.W., Sim, W. and Kim, J.S. (2004) *J. Org. Chem.*, **69**, 2877–2880.

13 (a) Zyryanov, G.V., Kang, Y. and Rudkevich, D.M. (2003) *J. Am. Chem. Soc.*, **125**, 2997–3007. (b) Kang, Y. and Rudkevich, D.M. (2004) *Tetrahedron*, **60**, 11219–11225.

14 Kang, Y., Zyryanov, G.V. and Rudkevich, D.M. (2005) *Chem. Eur. J.*, **11**, 1924–1932.

15 (a) Zyryanov, G.V. and Rudkevich, D.M. (2004) *J. Am. Chem. Soc.*, **126**, 4264–4270. (b) Sgarlata, V., Organo, V.G. and Rudkevich, D.M. (2005) *Chem. Commun.*, 5630–5632.

16 Organo, V.G., Leontiev, A.V., Sgarlata, V., Dias, H.V.R. and Rudkevich, D.M. (2005) *Angew. Chem. Int. Ed.*, **44**, 3043–3047.

17 Organo, V.G., Sgarlata, V., Firouzbakht, F. and Rudkevich, D.M. (2007) Chem. Eur. J., **13**, 4014–4023.

18 Wanigasekara, E., Leontiev, A.V., Organo, V.G. and Rudkevich, D.M. (2007) *Eur. J. Org. Chem.*, 2254–2256.

19 Dalgarno, S.J., Cave, G.W.V. and Atwood, J.L. (2006) *Angew. Chem. Int. Ed.*, **45**, 570–574.

20 Mansikkamaki, H., Busi, S., Nissinen, M., Ahman, A. and Rissanen, K. (2006) *Chem. Eur. J.*, **12**, 4289–4296.

21 (a) Hong, B.H., Lee, J.Y., Lee, C.-W., Kim, K.C., Bae, S.C. and Kim, K.S. (2001) *J. Am. Chem. Soc.*, **123**, 10748–10749. (b) Hong, B.H,. Bae, S.C., Lee, C.-W., Jeong, S. and Kim, K.S. (2001) *Science*, **294**, 348–351. (c) Kim, K.S., Suh, S.B., Kim, J.C., Hong, B.H., Lee, E.C., Yun, S., Tarakeshwar, P., Lee, J.Y., Kim, Y., Ihm, H., Kim, H.G., Lee, J.W., Kim, J.K., Lee, H.M., Kim, D., Cui, C., Youn, S.J., Chung, H.Y., Choi, H.S., Lee, C.-W., Cho, S.J., Jeong, S. and Cho, J.-H. (2002) *J. Am. Chem. Soc.*, **124**, 14268–14279.

22 Palmer, L.C. and Rebek, J. Jr. (2004) *Org. Biomol. Chem.*, **2**, 3051–3059.